B.Comp. Dissertation

Data-driven and Physics-inspired Machine Learning: Benchmarking quantum-inspired quadratic unconstrained binary optimization solvers

By

Guo Yulong

Department of Computer Science

School of Computing

National University of Singapore

2023/2024

B.Comp. Dissertation

Data-driven and Physics-inspired Machine Learning: Benchmarking quantum-inspired quadratic unconstrained binary optimization solvers

By

Guo Yulong

Department of Computer Science

School of Computing

National University of Singapore

2023/2024

Project No: H0811550
Advisor: Assoc Prof Stéphane Bressan

Deliverables:
Report: 1 Volume

Abstract

The quadratic unconstrained binary optimization (QUBO) problem represents a cornerstone in the field of combinatorial optimization that encapsulates a variety of scientific and industrial optimization problems. However, the QUBO problem is NP-hard and is traditionally extremely difficult to solve efficiently due to the exponentially increasing search space. In our work, we aim to measure the performance of different quantum-inspired QUBO solvers that utilize quantum effects to search for optimal solutions. We benchmark the D-Wave Quantum Annealer, Neural Network Quantum States (NNQS), and Quantum Approximate Optimization Algorithm (QAOA) solvers with classical commercial QUBO solvers. We use a dataset with a variety of combinatorial problems—not-all-equal 3-satisfiability, max-cut, and the Sherrington-Kirkpatrick model (SK model), and the solvers will be evaluated based on the average normalized energy and success probability. Our results show that the D-wave and NNQS solvers outperform the QAOA solver but are not able to match the performance of commercial QUBO solvers. We further investigate the performance of the NNQS solver when using different architectures and training algorithms. We find that the NNQS with a Restricted Boltzmann Machine with a continuous training algorithm gives the best performance across all datasets.

Subject Descriptors:

10002950.10003714.10003716.10011136 Mathematics of computing Discrete optimization
10010405.10010432.10010441 Applied computing Physics
10010147.10010257.10010293.10010294 Neural networks

Keywords:

Quadratic unconstrained binary optimization, Ising model, Quantum annealing, Neural network quantum states, Quantum Approximate Optimization Algorithm

Implementation Software and Hardware:

Linux, GPUs, Tesla A100, Python, Tensorflow, Dimod, Qiskit

Acknowledgement

I would like to thank my friends and family for their support during the project. I would also like to thank my project advisor Associate Professor Stéphane Bressan, research fellow Lu Jianlong, and past and present members of the research group for their invaluable guidance and support.

List of Figures

List of Tables

Table of Contents

Chapter 1

Introduction

1.1 Motivation

The quadratic unconstrained binary optimization (QUBO) problem arises in many types of combinatorial optimization tasks and has vast applications in both operational research and industry (Kochenberger, Hao, Glover, Lewis, Lu, Wang, & Wang, 2014). Problems that involve choosing a set of binary decisions to optimize an objective function can usually be expressed as a QUBO problem. Examples include the max-cut problem, knapsack problem, or even problems with more complex constraints such as the traveling salesman problem (Lucas, 2014). However, QUBO problems are NP-hard and are extremely hard to solve efficiently (Barahona, 1982Kochenberger et al., 2014). Traditionally, QUBO-solving methods are specialized for a specific problem domain in order to leverage the unique characteristics of each problem domain, limiting the versatility and portability of QUBO-solving methods (Glover, Kochenberger, Hennig, & Du, 2022).

The QUBO problem shares similarities with the Ising model in Physics, where variables are expressed as either -1 or 1, instead of the binary variables used in QUBO. The two models are equivalent and the correspondence between the QUBO problem and the Ising

model has opened the doors to solving QUBO problems with quantum computational methods (Glover et al., 2022). The equivalence not only enhances the problem domains that could be modeled as QUBO problems but also allows for the QUBO problem to be solved by more general quantum-inspired solving methods (Glover et al., 2022).

With a broad range of classical and quantum-inspired methods available to tackle QUBO problems, it is imperative to consolidate and benchmark existing QUBO-solving solvers to highlight their strengths and weaknesses for solving different kinds of QUBO problems.

1.2 Objectives

In the first section of the report, we aim to measure the performance of 3 quantum-inspired QUBO-solving solvers:

1. Quantum Annealing
2. Neural Network Quantum States
3. Quantum Approximate Optimization Algorithm

For comparison with quantum-inspired solvers, we will also use classical solvers as a baseline. We will explore 2 classical solvers:

4. Fixstars Amplify QUBO Solver
5. GUROBI Optimizer

For each solver, we will measure the success rate (probability of solving optimally) and normalized energy (relative performance of candidate solution) across QUBO problems of different types and sizes. More details of the solvers and performance metrics are available in chapter 3 and chapter 4. The results of the study will allow us to understand the current state of quantum-inspired QUBO solvers and how they compare to classical solvers.

In the second section of the report, we will further explore how Neural Network Quantum States can be used to simulate the quantum annealing process to solve QUBO problems. We conduct a systematic comparison of 2 neural network architectures and 3 different training algorithms highlighted in chapter 6 for Neural Network Quantum States.

The results of the study will allow us to better understand the current landscape of these quantum-inspired QUBO solvers and how they compare to the state-of-the-art classical commercial solvers.

Chapter 2

Background and Preliminaries

2.1 Quadratic unconstrained binary optimization

The quadratic unconstrained binary optimization (QUBO) problem is usually defined as

$$\arg\min_{x \in \{0,1\}^n} x^\intercal Q x \tag{2.1}$$

where $Q \in \boldsymbol{M}_{n \times n}(\mathbb{R})$ is an upper triangular square matrix with real coefficients and x is a binary input vector (Kochenberger et al., 2014). The matrix Q characterizes the QUBO problem and can be thought of as a way of representing the QUBO problem. $x^\intercal Q x$ is also known as the objective function for the problem. Some characteristics of QUBO problems are summarised below:

- The possible input space grows exponentially with the size of the problem n and makes the QUBO problem NP-hard and difficult to solve efficiently.
- In general, the solution of a QUBO problem does not need to be unique as multiple input x's can produce the same objective value.
- The objective function $x^\intercal Q x$ can also be expressed as $\sum_{i=1}^{n} \sum_{j=1}^{n} Q_{ij} x_i x_j$ which intuitively means that we sum up the coefficients Q_{ij} where both x_i and x_j are 1.

- The density d of a QUBO problem refers to the number of non-zero elements above the main diagonal of Q (quadratic terms) divided by the total number of elements above the main diagonal.
- We can also express a QUBO problem as a maximization problem by using finding $\arg\max_{x\in\{0,1\}^n} -x^\intercal Q x$.

Problems that are concerned with finding the best set of binary decisions to optimize an objective function can generally be formulated as a QUBO problem (Glover et al., 2022). Thus, the QUBO problem model has applications in a wide range of combinatorial optimization problems such as Max-Cut (Kochenberger, Hao, Lu, Wang, & Glover, 2013), number partitioning (Alidaee, Glover, Kochenberger, & Rego, 2005), and machine scheduling problems (Alidaee, 2009).

Once an optimization problem is expressed in a QUBO format, we can utilize general QUBO-solving methods to efficiently obtain solutions to the original problem without specializing in a particular problem domain (Kochenberger et al., 2014). The following sections will describe multiple examples of QUBO problems and reformulations.

2.1.1 Example QUBO problem

Consider the objective function

$$f(x_1, x_2, x_3) = -8x_1 + 6x_2 + 3x_3 - 2x_1x_2 + 4x_2x_3 \tag{2.2}$$

where $x_1, x_2, x_3 \in \{0, 1\}$ and we want to minimise f over all possible (x_1, x_2, x_3) (if we wanted to maximise f instead we can simply multiply all the coefficients of f by -1). Since the variables are binary, $x_i^2 = x_i$ for all i, we can redefine the objective function as

$$f(x) = x^\intercal Q x, \text{ where } x = \begin{bmatrix} x_1 \\ x_2 \\ x_3 \end{bmatrix}, \; Q = \begin{bmatrix} -8 & -2 & 0 \\ 0 & 6 & 4 \\ 0 & 0 & 3 \end{bmatrix} \tag{2.3}$$

The coefficients for Q_{ii} are equal to the coefficient of x_i in the original objective function while the coefficient for Q_{ij} where $i < j$ is the coefficient of $x_i x_j$ while the coefficients in the lower triangular portion of Q is 0. This is a simple QUBO problem and can be solved by enumerating all the possible inputs to obtain the optimal solution of $x_1 = 1, x_2 = 0, x_3 = 0$, and $f(1, 0, 0) = -8$.

2.1.2 Knapsack problem

In this section, we give an example of how a combinatorial optimization problem with inequality constraints can be formalized as a QUBO problem. The knapsack problem is a classic combinatorial optimization problem where we have a knapsack with integer weight capacity $W > 0$ and n items each having a weight $w_i > 0$ and profit $c_i > 0$. The problem seeks to find the optimal set of items to place in the knapsack to maximize total profit while not exceeding the knapsack weight limit. Formally, we have

$$\max \sum_{i=1}^{n} c_i x_i \tag{2.4}$$

$$\text{st.} \sum_{i=1}^{n} w_i x_i \leq W \tag{2.5}$$

$$x_i \in \{0, 1\}^n$$

The quantity 2.4 refers to the total profit of the chosen items and constraint 2.5 keeps the total weight below the weight limit. To convert this optimization problem into a QUBO problem, we can include the inequality constraint in our QUBO formulation by introducing slack variables, y_j's, which turn the inequality constraint into an equality

constraint (Quintero & Zuluaga, 2022).

$$\max \sum_{i=1}^{n} c_i x_i \tag{2.6}$$

$$\text{st.} \sum_{i=1}^{n} w_i x_i = \sum_{j=1}^{W} j y_j \tag{2.7}$$

$$\sum_{j=1}^{W} y_j = 1 \tag{2.8}$$

$$x \in \{0,1\}^n, y \in \{0,1\}^W$$

The slack variables y_j track the total weight of the knapsack with $y_j = 1 \Leftrightarrow$ total weight is j. Constraint 2.8 ensures that only one of y_j is equal to 1. With penalty parameters $C_1 > \sum_{i=1}^{n} c_i$ and $C_2 > \sum_{i=0}^{n} c_i$, we can formulate the following QUBO problem:

$$\max f(x,y) \coloneqq \sum_{i=1}^{n} c_i x_i - C_1 P_w^2 - C_2 P_n^2 \tag{2.9}$$

$$P_w \coloneqq \sum_{i=1}^{n} w_i x_i - \sum_{j=1}^{W} j y_j \tag{2.10}$$

$$P_n \coloneqq 1 - \sum_{j=1}^{W} y_j \tag{2.11}$$

$$x \in \{0,1\}^n, y \in \{0,1\}^W$$

Since the penalty parameters are chosen to be larger than $\sum_{i=1}^{n} c_i$, the optimal solution to the QUBO problem must have $P_w = P_n = 0$. Hence, ensuring that exactly one of the $y_i = 1$ and the total weight is below the knapsack capacity. Since the optimal solution to the original knapsack must also have a total weight below the knapsack capacity, the value of x that solves the QUBO must also solve the original knapsack problem. We can also formulate this QUBO problem in terms of Q by following similar steps as subsection 2.1.1.

2.1.3 Practical applications

There are numerous practical scenarios where QUBO formulations can be utilized.

- (Yarkoni, Huck, Schuelldorf, Speitkamp, Tabrizi, Leib, Back, & Neukart, 2021) uses real-world data of the location of DB Schenker shipping hubs in Europe to solve the shipment rerouting problem which aims to reduce the total distance traveled to fulfill a set of shipments.

- (Lang, Zielinski, & Feld, 2022) uses a QUBO formulation to solve portfolio optimization problems using real-world stock data sets of the New York Stock Exchange.

- (Tavares, 2008) formulates an image binarization method as a QUBO problem where the objective is to segment an image into its foreground and background which has further possible medical applications to improve x-ray imaging.

These practical applications of the QUBO problem motivate further exploration into different ways that QUBO problems can be solved efficiently which are explained further in chapter 3.

2.2 The Ising Model

The Ising model in Physics, proposed by Ernst Ising in 1925, can be thought of as a model of a magnet (Ising, 1925) and has been widely studied in Physics for its phase transition properties (Cipra, 1987). The Ising model serves as the bridge that allows for QUBO problems to be solved with quantum-based methods (Lucas, 2014). In the classical Ising model, a magnet consists of n molecules that are 'constrained to lie on the sites of a regular lattice' (Baxter, 2016). Each molecule i can be treated as a 'microscopic magnet' that points along some axis and has a 'spin' (s_i) that is either $+1$ (parallel to the axis) or -1 (anti-parallel to the axis). With n particles, the system can then have 2^n states, each corresponding to a configuration of the individual molecule spins.

2.2.1 Ising Hamiltonian

In quantum mechanics, the Hamiltonian of a system $\hat{H}$, is a linear operator that represents the total energy of a system and is a key component that governs the evolution of the system (Griffiths & Schroeter, 2018). Section 2.4 discusses the Hamiltonian and general quantum mechanics in greater detail. For this study, we can treat the Hamiltonian as a function of the quantum system that maps a quantum state to an energy level. The possible energy levels of the system are exactly the eigenvalues of its Hamiltonian and the corresponding eigenvectors are the possible states that are mapped to the certain energy level (Zen, My, Tan, Hébert, Gattobigio, Miniatura, Poletti, & Bressan, 2020).

In the Ising model with n particles, the Hamiltonian has two components — the external field term (characterized by $\mathbf{h} = (h_1, h_2, ..., h_n) \in \mathbb{R}^n$) and the interaction term between molecules (characterized by a strictly upper triangular matrix $\mathbf{J} \in \boldsymbol{M}_{n\times n}(\mathbb{R})$) (Lucas, 2014). We can express the Hamiltonian as a function of the n spins from each particle:

$$\hat{H}(s) = \hat{H}(s_1, s_2, ..., s_n) = -\sum_{1\leq i<j\leq N} J_{ij}s_is_j - \sum_{i=1}^{N} h_is_i \tag{2.12}$$

We can view $\mathbf{h}$ as the interaction of each particle with an external magnetic field and $\mathbf{J}$ as the coupling between pairs of spins. A positive J_{ij} term means that the energy is low when spins s_i and s_j are aligned while a negative J_{ij} term means that the energy is low when the spins are anti-aligned. A large value of h_i means that the spin s_i tends to be aligned or anti-aligned with an external magnetic field in the ground state. The Ising model was initially proposed to study phase transitions of the system at certain critical temperatures by solving for the ground state of the system at different temperatures (Ising, 1925). To find the ground state—the state of spins that minimizes the total system energy of the Ising model—we have to solve for $\arg\min \hat{H}(s)$ for $s \in \{0, 1\}^N$. This is equivalent to a corresponding QUBO problem up to a change in the variable domain (from spins to binary variables). The equivalence of the QUBO problem and the Ising model is one of the most significant applications of QUBO (Glover et al., 2022). We will show in the

following subsections how we can convert a QUBO problem into an Ising model and vice versa.

2.2.2 Converting QUBO to Ising

Given a QUBO problem with QUBO matrix Q, we can use the conversion, $x_i = \frac{s_i+1}{2}, s_i \in \{-1, 1\}$ to change the spin variables into binary variables. The objective function $f(x)$ of the QUBO problem can be expressed as

$$\begin{aligned} f(x) &= f(x_1, ..., x_n) \\ &= \sum_{1 \leq i < j \leq n} Q_{ij}(x_i x_j) + \sum_{i=1}^{N} Q_{ii} x_i \\ &= \sum_{1 \leq i < j \leq n} \frac{1}{4} Q_{ij}(s_i + 1)(s_j + 1) + \sum_{i=1}^{N} \frac{1}{2} Q_{ii}(s_i + 1) \end{aligned}$$

If we group the constant terms into k and let $a_i = \sum_{1 \leq j \leq N, j \neq i} \frac{1}{4} Q_{\min(i,j)\,\max(i,j)} + \frac{1}{2} Q_{ii}$, we can express the objective function as:

$$f(x) = \sum_{1 \leq i < j \leq n} \frac{1}{4} Q_{ij} s_i s_j + \sum_{i=1}^{N} a_i s_i + k$$

Removing the constant k which is irrelevant for optimization, we can reformulate the QUBO problem as an Ising model with $h_i = -a_i$ and $J_{ij} = -\frac{1}{4} Q_{ij}$ for $i \neq j$. Finding the ground state for the Ising model is the same problem as finding $\arg\min_{x \in \{0,1\}^n} x^\intercal Q x$, and the solution to the ground state of the Ising model can be mapped to a solution for QUBO problem using $x_i = \frac{s_i+1}{2}$. However, note that the optimal objective function value may be different due to the constant k.

2.2.3 Converting Ising to QUBO

Given the Hamiltonian of an Ising problem, we use the conversion $s_i = 2x_i - 1, x_i \in \{0, 1\}$ to change the spin variables into binary variables:

$$\begin{aligned}\hat{H}(s) &= -\sum_{1\leq i<j\leq n} J_{ij}s_is_j - \sum_{i=1}^{N} h_is_i \\ &= -\sum_{1\leq i<j\leq n} J_{ij}(2x_i - 1)(2x_j - 1) - \sum_{i=1}^{N} h_i(2x_i - 1) \\ &= -\sum_{1\leq i<j\leq n} J_{ij}(4x_ix_j - 2x_i - 2x_j + 1) - \sum_{i=1}^{N}(2h_ix_i - h_i)\end{aligned}$$

If we group the constant terms into k and let $a_i = 2h_i + \sum_{1\leq j\leq N, j\neq i} 2J_{\min(i,j)\,\max(i,j)}$, we can express the Hamiltonian as:

$$\hat{H}(s) = -\sum_{1\leq i<j\leq n} 4J_{ij}x_ix_j - \sum_{i=0}^{N} a_ix_i + k$$

Removing the constant k which is irrelevant for optimization, we can reformulate the Ising model Hamiltonian as a QUBO matrix Q such that $Q_{ii} = -a_i$ and $Q_{ij} = -4J_{ij}$ for $i < j$. Finding $\arg\min_{x\in\{0,1\}^n} x^\intercal Qx$ is now the same problem as finding the ground state for the original Ising model and the solution to the ground state of the Ising model can be mapped to a solution for QUBO problem using $s_i = 2x_i - 1$. However, note that the optimal objective function value may be different due to the constant k.

2.3 Solving for the ground state of the Ising model

In one and two-dimensional Ising models, where each particle can only interact with two or four direct neighbors, the ground state can be solved through exact methods such as calculating the partition function (Onsager, 1944) or using the transfer matrix method (Kramers & Wannier, 1941). However, when solving for the ground state of higher dimension Ising models, which are those that we are interested in, exact methods are computationally intractable for large systems since the computational resources scale

exponentially with the number of spins (Barahona, 1982). However, there are ways to approximate the ground state such as with the Metropolis-Hastings algorithm (Hastings, 1970) which can be used to increase the probability of finding the ground state of the system. More details for methods of solving Ising models that have higher dimensions can be found in chapter 3.

2.4 Wave functions, Observables and Ansatzes

Quantum physics is built around wave functions and operators (Griffiths & Schroeter, 2018). Wave functions represent the state of the system and live in a Hilbert space, which is the set of all square-integrable functions:

$$f(x) \text{ such that } \int_{-\infty}^{\infty} |f(x)|^2 \, dx < \infty$$

This is generally an infinite dimensional complex vector space and allows for the wave function, denoted as Ψ, to be normalized so that $\int_{-\infty}^{\infty} |\Psi|^2 \, dx = 1$. Under the statistical interpretation of quantum mechanics, $|\Psi(x)|^2$ would also represent the probability of a system being in state x once it is measured. This also means that a wave function can exist as a superposition of states. For this project, we will adopt the statistical interpretation and view the wave function as simply a probability distribution over all possible state configurations.

Quantum operators represent the observables—measurable quantities of the system such as position, momentum, or energy. Quantum operators are hermitian linear operators that act on a wave function to map states to real values. The eigenvalues of the operator have to be real as they correspond to one of the possible measured values of the represented quantity. When an operator acts on a wavefunction that exists as a superposition of multiple states, it returns an expected value of the observable instead. The Hamiltonian, which is the energy operator, is the main operator used in this study and the set of

eigenvalues of the Hamiltonian are all the possible energies that the system could have.

For an Ising model, the wavefunction encodes the probabilities of each configuration of spins and the Hamiltonian maps each wavefunction to an energy level. If a wave function only has one possible configuration, the Hamiltonian will return the eigenvalue that matches the energy level of the state. If the wave function is in a superposition of states, the Hamiltonian will return a linear combination of the eigenvalues instead.

An Ansatz is an educated guess for the solution to a problem and often involves a reduction in the complexity or size of the problem (Blekos, Brand, Ceschini, Chou, Li, Pandya, & Summer, 2023). When solving for the ground state of a wave function with variational methods, an Ansatz is used to represent a subspace of the infinite-dimensional Hilbert space that the wave function lives in. It is important to ensure that the wave function is general enough to closely approximate the space of all solutions yet is specific enough to be computed.

2.5 Sampling methods

Both Gibbs and Metropolis-Hasting (MH) sampling are Markov Chain Monte Carlo (MCMC) sampling methods and are used to sample from a probability distribution $\mathbb{P}(X)$ when direct sampling is difficult. We will first introduce MH sampling and then Gibbs sampling as a special case of MH sampling.

Metropolis-Hasting sampling

Metropolis-Hasting sampling (Hastings, 1970) proceeds as follows:

1. Initialise the system with a random sample $\mathbf{x}$
2. Draw new candidate x^* from $q(x^*|x)$.
3. Accept the new candidate by replacing $\mathbf{x} \leftarrow x^*$ with probability $\alpha = \min\left(1, \frac{\mathbb{P}(x^*)/q(x^*|x)}{\mathbb{P}(x^*)/q(x^*|x)}\right)$.

4. Repeat steps 2 and 3 for a certain number of iterations or until $\mathbf{x}$ fulfills some convergence criteria.

Gibbs sampling

Gibbs sampling (Geman & Geman, 1984) is used when directly sampling from the joint distribution $\mathbb{P}(X)$ is difficult but sampling from the separate conditional distributions is more practical. It proceeds as follows:

1. Initialise the visible layer of the RBM with a random sample $\mathbf{s}$.
2. Update the hidden layer by sampling from their respective conditional probability distribution given the current visible layer configuration.
3. Update the visible layer by sampling from their respective conditional probability distribution given the current hidden layer configuration.
4. Repeat steps 2 and 3 for a certain number of iterations or until $\mathbf{s}$ fulfills some convergence criteria.

The Gibbs sampling method can be seen as a special case of MH sampling where we have $\alpha = 1$ and thus always accept the new candidate sample. The key benefit of Gibbs sampling on a RBM is that the visible units are conditionally independent given the hidden layer and the hidden units are similarly conditionally independent given the visible layer. Thus the sampling can be easily parallelized and accelerated using GPUs.

Chapter 3

Methods for solving QUBO problems

This chapter reviews the different approaches that are used to solve QUBO problems along with their advantages and limitations.

There are a variety of possible methods for solving QUBO problems and Ising models which can be broadly categorized as Classical, Quantum Annealing, Neural Network Quantum States, and Hybrid Quantum-Classical Algorithms.

3.1 Classical

Classical approaches search for solutions without exploiting quantum properties such as the superposition of states. A typical classical approach to solving large QUBO problems is by exact diagonalization of the corresponding Ising Hamiltonian (Zen, 2021). Exact diagonalization solves for all the eigenvalues and eigenvectors by diagonalizing the corresponding Ising Hamiltonian matrix. This is also known as the eigendecomposition of a matrix and is possible for all Hermitian matrices, which are those that represent the Hamiltonian of a quantum system (Horn & Johnson, 1990). However, the runtime of exact diagonalization scales exponentially with input problem size and becomes computation-

ally infeasible once the matrix grows large (Zen, 2021). Since we are only interested in finding the smallest eigenvalue and the corresponding eigenvector, we can use iterative methods such as the Lanczos algorithm or the implicitly restarted Arnoldi method to find the smallest eigenvalue (Lanczos, 1950Lehoucq, Sorensen, & Yang, 1998). However, such methods also often run into stability issues. The rapidly increasing search space for QUBO problems has inspired classical methods that aim to efficiently find approximate solutions to QUBO problems instead.

One class of such methods relies on "heuristics" to search for optimal solutions (Dunning, Gupta, & Silberholz, 2018). For example, variants of Tabu search—a local search algorithm that allows for moves that are not improvements and discourages visiting already visited states—are highly competitive heuristic algorithms to find good solutions to QUBO problems(Kochenberger et al., 2013Palubeckis, 2006). Dunning et al.(2018) conducted a systematic review and evaluation of published heuristics for QUBO problems and provided an open-source problem repository MQLib for further research.

Another classical approximate method for solving QUBO problems is simulated annealing (SA) (Katayama & Narihisa, 2001). Simulated annealing (Kirkpatrick, Gelatt, & Vecchi, 1983) is a probabilistic method for approximating the global minimum of a function. The main idea of SA is to start with an initial trial state and a temperature T which decreases slowly during the search. In each iteration, the algorithm samples neighboring solutions of the current state and probabilistically accepts the new state based on the difference in energy, ΔE, between the current state and the new state. If $\Delta E < 0$, then the new state is always accepted and if $\Delta E \geq 0$, the new solution is accepted with probability $\propto e^{-\frac{\Delta E}{T}}$. The algorithm to sample new states is adapted from the Metropolis-Hastings sampling method (Hastings, 1970) and the chance to explore poorer solutions allows for the algorithm to escape local minima.

There are many more classical approaches to solving QUBO problems as it has been

studied extensively. For a detailed survey of classical methods for solving QUBO problems, refer to (Punnen, 2022).

3.2 Quantum Annealing

Quantum annealing, first formulated by Kadowaki and Nishimori (1998), can solve for the ground state configuration of Ising models by utilizing the *adiabatic theorem*. The *adiabatic theorem* states that "a quantum system in its ground state will remain in the ground state, provided that the Hamiltonian governing the dynamics changes sufficiently slowly" (Yarkoni, Raponi, Back, & Schmitt, 2022Born & Fock, 1928). If we can manipulate the final Hamiltonian of a quantum system to one that describes the Ising model of interest, we can find the ground state of the Ising model simply by measuring the final configuration of the quantum system.

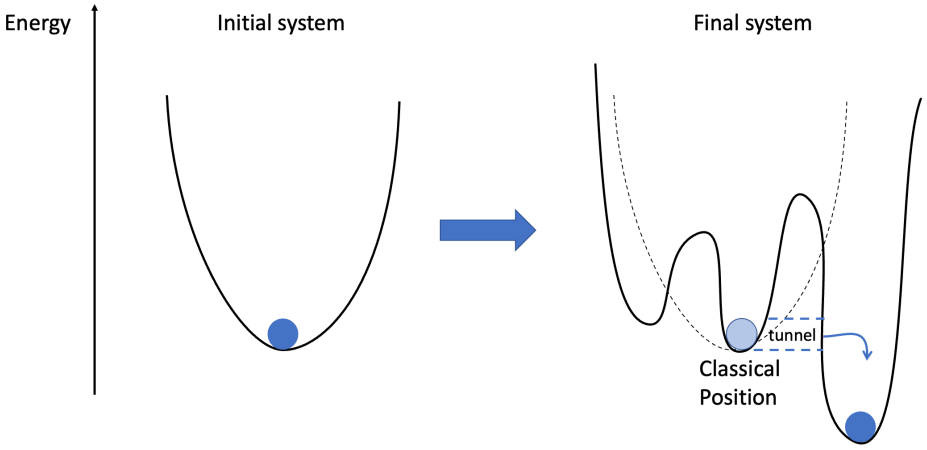

Figure 3.1: Energy landscape before (left) and after (right) quantum annealing

Quantum annealers first prepare a system in the ground state with a simple initial Hamiltonian H_0 (called the mixer or tunneling Hamiltonian), shown with a simple energy landscape in the left of Figure 3.1. Then, the system Hamiltonian is slowly changed to a more complex form H_c (Lucas, 2014), shown with a complex energy landscape in the

right of Figure 3.1. The Hamiltonian at any point $H(s)$ can be written as

$$H(s) = A(s)H_0 + B(s)H_c \tag{3.1}$$

where $s \in [0, 1]$ is the normalized anneal fraction and $A(s)$ and $B(S)$ are decreasing and increasing functions respectively and are determined by the specific quantum annealing controls. At the start of the annealing we should have $A(s) >> B(s)$ and at the end of the annealing we should have $B(s) >> A(s)$. If the transition time is sufficiently large, the adiabatic theorem ensures that the system will remain in the ground state which can then be measured to yield the desired ground state configuration of H_c (Yarkoni et al., 2022).

As H_0 usually consists of a transverse magnetic field and does not commute with the target Hamiltonian H_c, it allows for quantum tunneling through energy barriers between classical states (Kadowaki & Nishimori, 1998). This allows for the wave function to remain at the ground state even when classical search methods may end up stuck in a local minimum. However, the adiabatic theorem requires an arbitrarily long anneal time to guarantee that the system remains in the ground state which is not feasible for practical purposes. Current implementations of quantum annealing instead rely on a finite time approximation with repeated sampling to increase the success rate (Farhi, Goldstone, Gutmann, Lapan, Lundgren, & Preda, 2001).

Quantum annealing has been extensively studied and applied in multiple fields such as Scheduling Problems (Rieffel, Venturelli, O'Gorman, do, Prystay, & Smelyanskiy, 2014), Portfolio Optimization (Rosenberg, Haghnegahdar, Goddard, Carr, Wu, & Lopez de Prado, 2016) and Quantum simulations (Harris, Sato, Berkley, Reis, Altomare, Amin, Boothby, Bunyk, Deng, Enderud, Huang, Hoskinson, Johnson, Ladizinsky, Ladizinsky, Lanting, Li, Medina, Molavi, & Yao, 2018). Even though there are significant roadblocks in scaling the currently limited hardware capabilities (Yarkoni et al., 2022) and it is debated whether Quantum Annealing will run faster than classical search methods (Lucas, 2014), there is

hope that these challenges can be tackled soon with the rapid progress made in quantum computing research. At present, the leading commercial provider of quantum annealing hardware is D-wave, a Canadian quantum computing company (D-Wave Systems, 2023).

3.3 Neural-Network Quantum States

Carleo and Troyer (Carleo & Troyer, 2017) introduced a neural-network-based method for modeling the wave function of a target quantum system known as *neural-network quantum states* (NNQS). The authors used the approach to find the ground state and time evolution of the Ising and Heisenberg models in Physics. The NNQS is used as an Ansatz to approximate the wave function, which can be viewed as a complex probability distribution, of a system as an artificial neural network (Zen, 2021). The more general method of using an Ansatz as a trial wave function and minimizing its energy through Monte Carlo sampling is also known as variational Monte Carlo (VMC).

The theoretical foundations of the ability of NNQS to approximate a wave function rely on the Kolmogorov–Arnold representation theorem (Kolmogorov, 1957), which implies that every multivariate, smooth function can be represented by a neural network with two hidden layers. Since the wave function of a quantum system generally satisfies these requirements, we can expect that a neural network can reasonably approximate the wave function of the system (Carleo & Troyer, 2017).

The original NNQS architecture utilized a Restricted Boltzmann Machine (RBM) as its network (Carleo & Troyer, 2017). The RBM, shown in Figure 3.3, is an energy-based generative model that has two layers of nodes, a visible layer $\boldsymbol{s}$ with n nodes, a hidden layer $\boldsymbol{h}$ with m nodes, and a weight matrix $\mathbf{W}$. The number of hidden nodes is generally a multiple of the number of visible nodes and the ratio $\alpha = \frac{m}{n}$ is a hyperparameter of the model. Each visible node s_i is connected to every hidden node h_j with a certain weight W_{ij} but there are no connections within the visible or hidden layer. In other words, the

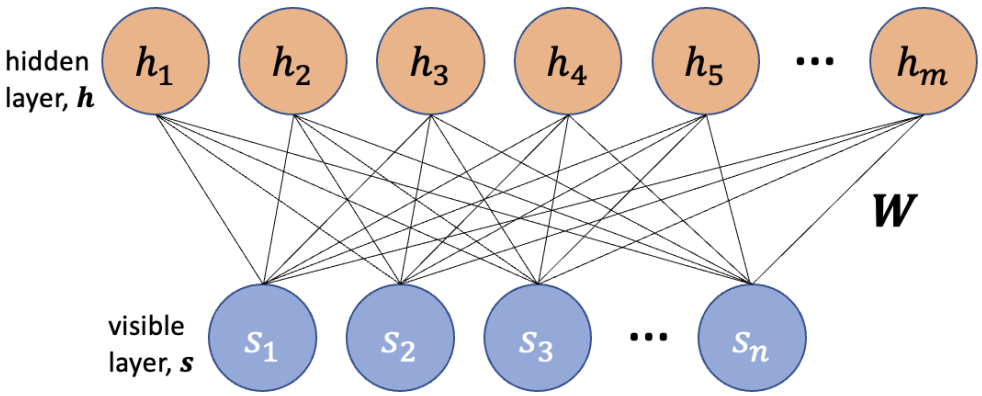

Figure 3.2: Structure of Restricted Boltzmann Machine

visible and hidden nodes of the RBM form a bipartite graph.

When approximating the wave function of an Ising model, each visible node s_i is used to represent the spin of a particle in the Ising model and can only take on the values of 1 and -1 (Carleo & Troyer, 2017). The representation of the wave function by the RBM can be expressed as:

$$\Psi(\boldsymbol{s};\boldsymbol{\theta}_{rbm}) = \sum_{h} e^{\sum_i a_s s_i + \sum_j b_j h_j + \sum_{i,j} W_i s_i h_j} \tag{3.2}$$

where $\boldsymbol{\theta}_{rbm} = \{\boldsymbol{a}, \boldsymbol{b}, \boldsymbol{W}\}$ are the biases and weights of the RBM (Carleo & Troyer, 2017). The RBM is trained in an unsupervised manner. The network weights $\mathbf{W}$ are usually updated by performing Gibbs sampling, calculating the average energy of sampled configurations, and using gradient-based optimization algorithms (Zen, 2021).

Other neural network architectures such as the Multilayer Perceptron (MLP) can also be used in NNQS. An MLP model is a feedforward artificial neural network that consists of an input layer $\boldsymbol{x}$, one or more hidden layers, and an output layer. Each layer is fully connected to the next layer with certain weights and each node has a non-linear activation function σ such as the sigmoid or ReLU function. Each input node x_i represents the spin of a particle in the Ising model and the output nodes represent the value of the wave function. If we assume that the wave function is real and positive, then only one output

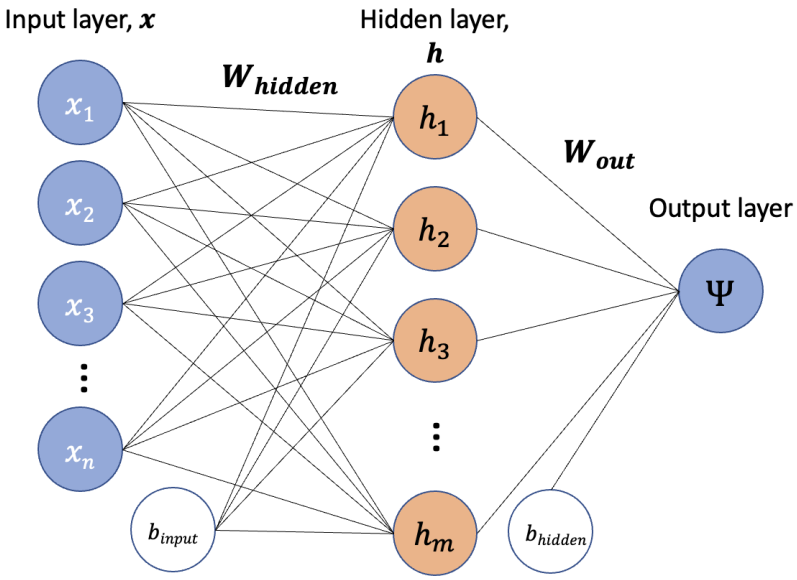

Figure 3.3: Structure of Multilayer Perceptron with 1 hidden layer and 1 real-valued output node

node is needed to represent the real part of the wave function. (Carleo & Troyer, 2017). With a complex wave function, we could employ output combinations with two nodes representing either the real and imaginary components or the magnitude and phase. With one hidden layer, the MLP representation of the wave function can be expressed as:

$$\Psi(\boldsymbol{x};\boldsymbol{\theta}_{mlp}) = \sigma_{out}\left(\boldsymbol{W}_{out}\,\sigma_{hidden}\left(\boldsymbol{W}_{hidden}\boldsymbol{x} + \boldsymbol{b}_{input}\right) + \boldsymbol{b}_{hidden}\right) \tag{3.3}$$

where $\boldsymbol{\theta}_{mlp} = \{\boldsymbol{W}_{hidden}, \boldsymbol{b}_{input}, \boldsymbol{W}_{out}, \boldsymbol{b}_{hidden}\}$ are the weights and bias of the MLP and $\sigma_{out}, \sigma_{hidden}$ are the non-linear activation functions of the nodes (Carleo & Troyer, 2017). The MLP is trained in an unsupervised manner, similar to the RBM, except that a more general sampling method, the Metropolis-Hasting algorithm, is used (Zen, 2021).

3.4 Hybrid quantum-classical

The fourth class of QUBO solving methods are hybrid quantum-classical methods which are designed to make use of current limited quantum computing resources by integrating

them with classic methods to solve combinatorial optimization problems (Zhou, Wang, Choi, Pichler, & Lukin, 2020). In the noisy intermediate-scale quantum (NISQ) era that we are currently in, quantum computers are not yet stable enough to be able to reliably run deep and complex quantum circuits.

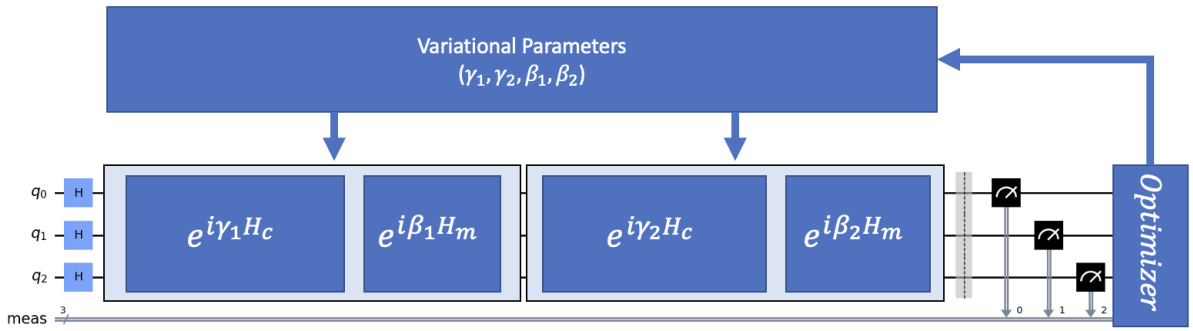

Figure 3.4: Circuit diagram of the QAOA algorithm circuit with $p = 1$

One such algorithm is the Quantum Approximate Optimization Algorithm (QAOA) which is used to find approximate solutions to general combinatorial optimization problems (Farhi, Goldstone, & Gutmann, 2014). Similar to NNQS, QAOA aims to find an approximation of the ground state of an input Hamiltonian using gate-based quantum circuits and $2p$ parameters which are optimized with a classical computer (Willsch, Willsch, Jin, De Raedt, & Michielsen, 2020). With a problem of size N. the algorithm first prepares a quantum state $|+\rangle^{\otimes N}$ in uniform superposition by applying the Hadamard gate to each of the n inputs (Willsch et al., 2020). The trial wave function is then constructed by

$$\Psi(\boldsymbol{\gamma}, \boldsymbol{\beta}) = U_B(\beta_p)U_C(\gamma_p)...U_B(\beta_1)U_C(\gamma_1)|+\rangle^{\otimes N} \tag{3.4}$$

$$U_C(\gamma) = e^{-i\gamma H_c}$$

$$U_B(\beta) = e^{-i\beta H_0}$$

Using the time-independent Schrödinger equation, we can see that U_c and U_B are operators that evolve the state with the Hamiltonian H_c (problem Hamiltonian) and H_0 (an easy-to-implement, mixing Hamiltonian) for time intervals $\boldsymbol{\gamma}$ and $\boldsymbol{\beta}$ while the parameter p

determines the number of independent parameters of the final state (Willsch et al., 2020). The state is then measured and $\boldsymbol{\gamma}$ and $\boldsymbol{\beta}$ are chosen to minimize the average energy of the sample measurements. With the optimal parameters, the final solution can then be determined by repeatedly sampling from the trial wave function.

There is evidence that QAOA is more difficult for classical computers to simulate compared to Quantum Annealing which may suggest that it could be a better way to demonstrate quantum supremacy (Farhi & Harrow, 2016). In contrast to quantum annealing which can only be run on specialized quantum annealing devices, QAOA can be implemented on a general gate-based quantum computer (Kurowski, Pecyna, Slysz, Rozycki, Waligora, & Weglarz, 2023).

Chapter 4

Methodology

This chapter explains the methodology employed in our study, which includes the solvers, datasets, and evaluation metrics.

4.1 Solvers

We will employ five QUBO-solving-methods:

1. D-Wave Quantum Annealing
2. Neural Network Quantum States (NNQS)
3. Quantum Approximate Optimization Algorithm (QAOA)
4. GUROBI Optimizer
5. Fixstars Amplify QUBO Solver

The following sections will provide more information on the solvers used for each method.

4.1.1 D-Wave Quantum Annealing

We will use quantum annealers from D-wave Systems as the solver for Quantum Annealing. D-Wave Systems, a Canadian-based company, currently produces the most popular

commercially available quantum annealing hardware and uses superconducting qubits to represent binary variables in their annealers (Yarkoni et al., 2022). Given a target QUBO problem to solve, the process for using a D-Wave Systems Quantum Processing Unit (QPU) is as follows:

1. **Problem Definition** QUBO problem is first converted to its corresponding Ising model Hamiltonian on the local device.

2. **Minor Embedding** As the Quantum Processing Unit (QPU) used by D-Wave is not fully connected as shown in Figure 4.1, a single variable in the Ising model may need to be represented by multiple qubits called a *chain* which are forced to return the same value with large interaction terms (D-Wave Systems, 2023). This will be done with an embedder provided by the D-wave library.

3. **Programming** The parameters of the annealing process are set, which consists of the bias for each qubit (represents magnetic field acting on each qubit) and coupler strength (represents variable interaction).

4. **Initialization** The QPU is initialized in the ground state of an easy-to-implement initial Hamiltonian. The qubits are prepared to be in a superposition of all possible states.

5. **Annealing** The system evolves with a time-varying Hamiltonian.

6. **Readout of solution** The spin values of the qubits are measured and stored as a possible solution.

7. **Resample** As the finite-time quantum annealing process does not guarantee that the system ends up in the ground state, we repeat the sampling to obtain many possible solutions that are likely to be the ground state of the initial Hamiltonian.

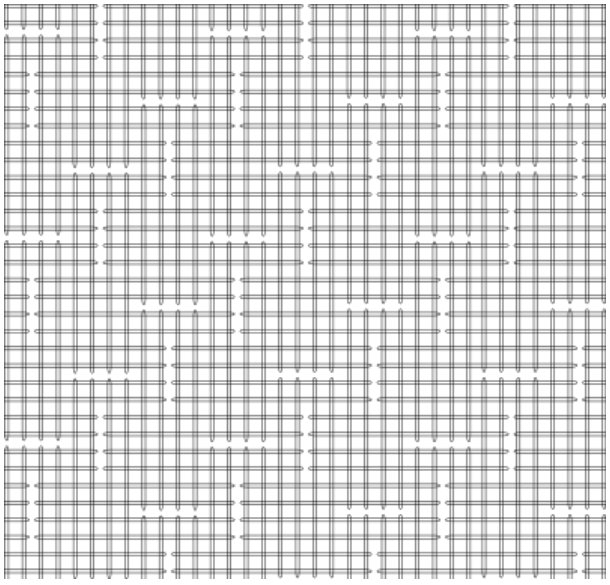

Figure 4.1: A view of the D-Wave pegasus topology where each line represents a qubit and intersections represent available couplers (McGeoch & Farré, 2021)

The experiments will be conducted with the D-Wave Advantage 4.1 QPU with up to 5640 qubits and 40484 couplers (McGeoch & Farré, 2021). The QPU operates at a temperature of approximately 12mK and is built with "a network of tunably coupled rf superconducting quantum–interference device (rf-SQUID) qubits" arranged with the Pegasus graph topology that allows for up to 15 couplers per qubit, shown in Figure 4.1. The system Hamiltonian as a function of s, the normalized anneal fraction, is:

$$H(s) = -\frac{A(s)}{2}\left(\sum_i \hat{\sigma}_x^{(i)}\right) + \frac{B(s)}{2}\left(\sum_i h_i \hat{\sigma}_z^{(i)} \ + \sum_{i>j} J_{i,j}\hat{\sigma}_z^{(i)}\hat{\sigma}_z^{j)}\right) \tag{4.1}$$

where functions $A(s)$ and $B(s)$ used in the Advantage 4.1 QPU are shown in Figure 4.2 with $A(s) >> B(s)$ when $s = 0$ and $B(s) >> A(s)$ when $s = 1$ and have an energy scale of around $10^{-24}J$. We will use the default annealing time of $20\mu s$ with 1000 repeated samplings (number of reads). The candidate solution will be taken as the best solution among the 1000 sampled configurations.

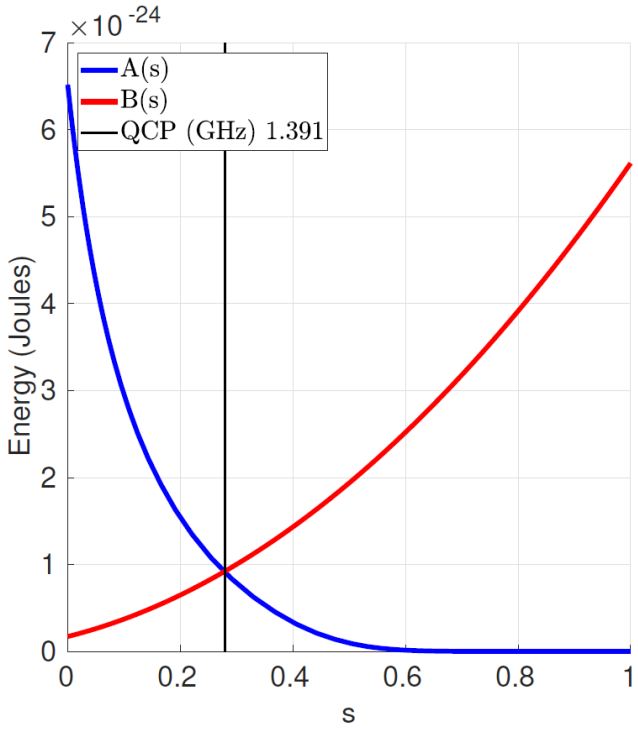

Figure 4.2: Annealing functions $A(s)$ and $B(s)$ as a function of the normalized anneal fraction s (McGeoch & Farré, 2021)

4.1.2 Neural-Network Quantum States

We will adopt the Python library MAPALUS for implementing the Neural-Network Quantum States (Zen, 2021). MAPALUS uses the Tensorflow library and enables parallel execution on general-purpose graphics processing units (GPUs) for quicker sampling. In this section, we will use the Restricted Boltzmann Machine (with $5n$ hidden nodes and the sigmoid activation function) as the underlying architecture for the NNQS.

To solve a given input QUBO problem, the NNQS will be used to simulate a quantum annealing process with a time-dependent Hamiltonian that follows Equation 3.1. Since the equations for $A(s)$ and $B(s)$ are not available, we employ a curve-fitting process to obtain analytical functions for use in the NNQS. The fitted functions used are $A(s) = 1.11e^{-7.06s} + -0.00569$ and $B(s) = 0.680s^2 + 0.288s + 0.0305$, details on the curve fitting process are available in Appendix A.

Algorithm 1 NNQS Progressive Training

Require: Problem Hamiltonian $\hat{H}_c$

Ensure: Trained NNQS

Initialize NNQS with random weights;

for $s \in [0.1, 1.0]$ step 0.1 **do**

Set $H(s) \leftarrow A(s)\hat{H}_0 + B(s)\hat{H}_c$;

Train NNQS on $H(s)$ until convergence or until epoch limit of 100 is reached;

The NNQS will be trained with a progressive training schedule that mimics the quantum annealing process and follows Algorithm 1. $\hat{H}_c$ is the problem Hamiltonian and $\hat{H}_0$ is a Hamiltonian with linear biases as 1 and no quadratic terms. The normalized anneal fraction s is increased in small steps while the NNQS is trained until convergence or until the epoch limit. This ensures that the NNQS remains in the ground state throughout the "annealing" process and that the problem Hamiltonian changes relatively slowly. Each training process runs for at most 1000 epochs and the model weights are updated with the RMSprop optimizer from the Tensorflow library and a learning rate of 0.001. The candidate solution will be taken as the best solution among the final 1000 sampled configurations from the respective sampling methods as outlined in section 2.5. All NNQS experiments were run with a 32 Core AMD EPYC 7543P Processor at 2.7GHz and an NVIDIA A100 40GB GPU with 500GB of RAM.

4.1.3 Quantum Approximate Optimization Algorithm

We will employ the implementation of QAOA in Qiskit with $p = 1$ using a backend hosted on the IBM Quantum Platform (IBMQ) (Qiskit contributors, 2023). Even though IBMQ allows for access to quantum computers with up to 127 qubits, it is highly limited with impractical wait times (> 5 hours for each problem) for a benchmarking experiment. Instead, we will be utilizing the IBMQ simulator, which is capable of handling quantum

circuits with up to 32 qubits. With an input Hamiltonian $\hat{H}_c$, we will use the default mixing Hamiltonian of $\hat{H}_0 = \sum_i \hat{\sigma}_x^{(i)}$ and a set of Hadamard gates applied to all qubits as the initial state. The Qiskit transpiler is used to optimize the decomposition of the operators into their individual parametrized quantum gates as shown in Figure 4.3 (IBM, 2024).

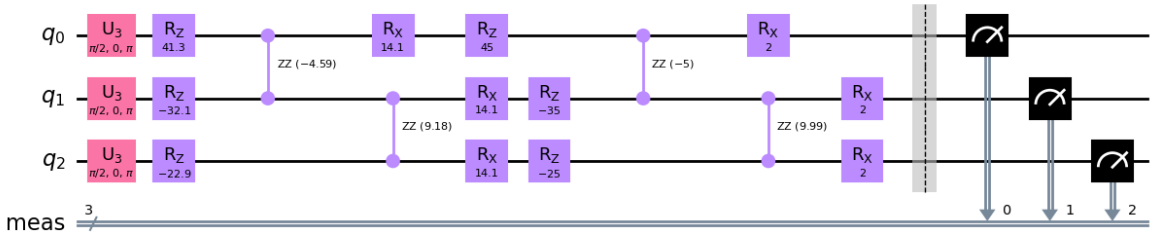

Figure 4.3: Circuit diagram with the Hadamard gates, problem Hamiltonian operator, and mixing Hamiltonian operator and (left to right)

The experiments were run on the IBMQ cloud with the ibmq_qasm_simulator, a general-purpose simulator for simulating quantum circuits, and the COBYLA optimizer for updating the circuit parameters. We will assume an ideal circuit without a quantum noise model for measuring the optimal performance of the QAOA algorithm. We will repeatedly sample the final circuit with optimized parameters for 1000 times and the candidate solution will be taken as the best solution among the sampled configurations.

4.1.4 GUROBI Optimizer

The GUROBI optimizer is used as a state-of-the-art classical commercial solver which is free for academic use (Gurobi Optimization, LLC, 2023). As the GUROBI optimizer supports QUBO problems, we construct the QUBO matrix directly using the Gurobi Python library and run the optimizer locally for 10 minutes for each input problem. If the optimizer finishes before the cutoff, the candidate solution is guaranteed to be the optimal configuration, otherwise, we would use the best solution found within the cutoff

time as a candidate solution. All experiments were run with a 32 Core AMD EPYC 7543P Processor at 2.7GHz and an NVIDIA A100 40GB GPU with 500GB of RAM using Gurobi Optimizer version 10.0.3.

4.1.5 Fixstars Amplify QUBO Solver

The Fixstar Amplify QUBO solver is a commercial simulated annealing-based QUBO solver that has limited free access (Dunning et al., 2018). As the Fixstar solver supports QUBO problems, we submit the QUBO matrix directly using the Fixstar API and run the solver with the highest allowed time limit which is 100 seconds for each input problem. The solver is implemented on GPUs and is run on Fixstar remote servers which are accessed with an API token.

4.2 Benchmark datasets

We use 3 randomly generated problem sets to benchmark our QUBO solvers. These problems were chosen as they are commonly used to represent NP-hard problems to measure the performance of QUBO solvers and are relatively straightforward to encode into QUBO form. They are the not-all-equal 3-satisfiability (NAE3SAT), max-cut, and the Sherrington-Kirkpatrick (SK) model. Each problem set comprises problems of 13 sizes, ranging from 10 to 300[1]. 20 different random problems are generated[2] for each problem size n for a total of 260 problems per problem set. Each problem is also first formulated in either the QUBO or Ising form and conversion between them follows subsection 2.2.2 and subsection 2.2.3.

[1] $n \in [10, 15, 20, 25, 30, 35, 50, 75, 100, 150, 200, 250, 300]$

[2] random seed is chosen to be from $0 - 19$

Not-all-equal 3-satisfiability (NAE3SAT)

The NAE3SAT problem is a variant of the boolean satisfiability problem where each problem instance consists of n boolean variables $(x_1, x_2, ..., x_n)$ and m clauses that each combine three literals which can be a variable or its negation. The objective is to find an assignment of boolean values such that the three values in each clause are not all the same, i.e., each clause has at least one true and one false value. The ratio of clauses to variables $\rho = \frac{m}{n}$ is a problem parameter and NAE3SAT problems are known to transition from being satisfiable to unsatisfiable at around $\rho = 2.1$ (Achlioptas, Chtcherba, Istrate, & Moore, 2001). We generate random NAE3SAT problems with $\rho = 2.1$ using the random_nae3sat generator from the dimod D-wave Python library which "randomly samples clauses from the space of 3-variable clauses with replacement" (Inc., 2024a).

To convert a NAE3SAT problem into an Ising problem, we represent each boolean variable as a spin variable and turn each clause into a Hamiltonian term. For example, for the clause $(x_1, x_2, \neg x_3)$, we use the Hamiltonian term $H(s_1, s_2, s_3) = s_1 \cdot s_2 + s_2 \cdot (-s_3) + s_1 \cdot (-s_3)$ which has a value of 3 when $x_1 = x_2 = \neg x_3$ and -1 otherwise. The final Hamiltonian $\hat{H}_c$ is simply a sum of the individual Hamiltonian terms for each clause.

Max-cut

The max-cut problem aims to find a partition of the vertices of a graph $G = (V, E)$ into V_0, V_1 with $V = V_0 \cup V_1$ and $V_0 \cap V_1 = \emptyset$, such that the number of edges crossing V_0 and V_1 is maximized. We will use the Erdos-Renyi model to generate random graphs with n vertices and a probability $p = 0.25$ to include each edge.

To convert a max-cut problem into a QUBO problem, we represent the assignment of each vertex as a binary variable ($x_v = i$ if $x \in V_i$) and use the objective function $f(\mathbf{x}) = \sum_{e=(u,v)\in E} -x_u - x_v + 2x_u x_v$, where each term has a value of -1 when $x_u \neq x_v$ and 0 otherwise. If a problem has a max-cut value of C, the objective function would

have a minimum value of $-C$.

Sherrington-Kirkpatrick (SK) model

The Sherrington Kirkpatrick (SK) model is an Ising problem with a random Hamiltonian of the form $\hat{H}_c = \frac{1}{\sqrt{n}} \sum_{1 \leq i < j \leq n} J_{ij} s_i s_j$ where $J_{ij} \sim \mathcal{N}(0, 1)$ are independent standard Gaussian variables. The energy landscape of the SK model is complex and has exponentially many local minima with a unique global minimum separated by high energy barriers (D. J. Thouless & Palmer, 1977). This many-valley structure implies that it is extremely difficult to find the exact solution of the model. We generate random Gaussian variables with a random normal generator from the NumPy Python library.

4.3 Performance evaluation

To evaluate the performance of each solver we will use two performance metrics:

1. The probability of finding the best solution. The best solution is one that has the same energy as the lowest energy among all solutions found by the 5 solvers. Since we are generating 20 problems of each type and size, the success probability for each solver is:

$$\bar{p} = \frac{\text{number of best solutions found}}{20} \tag{4.2}$$

2. The average normalized energy, used in (Willsch et al., 2020), which is:

$$\bar{r}_{solver} = \frac{1}{20} \sum_{i=1}^{20} \frac{E_{max} - E_{solver}}{E_{max} - E_{min}} \tag{4.3}$$

where E_{max} and E_{min} are the energies of the worst and best solutions found by all solvers and E_{solver} is the energy that the solver found. Note that if a solver finds the best solution it gets a normalized energy of 1 and if it finds the worst solution it gets a normalized energy of 0. All solvers get a normalized energy of 1 if all solutions have the same energy.

The average normalized energy reflects the quality of the solutions that the solvers produce, while the success probability measures the solvers's ability to find the best solution.

Chapter 5

Benchmarking QUBO solvers

This chapter first introduces related benchmarking work that has been done for QUBO problems and QUBO solvers. Then, we present our results for the solvers and datasets used for this study.

5.1 Related benchmarking work

One of the first benchmarking works for quantum annealing was conducted by Denchev et al. (2016), who measured the performance of D-Wave quantum annealing on the older D-Wave 2X machine using specially crafted problems that have tall and narrow energy barriers separating local minima. Quantum annealing is expected to be 1.8×10^8 times faster compared to simulated annealing, which tends to fail with problems with such an energy landscape.

Willsch et al. (2020) evaluated the performance of QAOA on the IBMQ backend and the D-Wave solver using instances of MaxCut and 2-satisfiability problems with up to 18 variables. The performance of the QAOA algorithm is inconsistent and underperforms quantum annealing in their problem set. More recently, Pelofske, Bärtschi, and Eidenbenz (2023) also compared the performance of QAOA on the IBMQ backend and D-Wave

quantum annealing on randomly generated Ising problems with cubic interaction terms and also found that quantum annealing had superior performance over QAOA for all problem sizes.

Gomes, McKiernan, Eastman, and Pande (2019) showed that the NNQS solving method with an RBM architecture produces good solutions for the max-cut problem with graph sizes of up to 256. Khandoker, Abedin, and Hibat-Allah (2023) uses recurrent neural networks as the NNQS architecture for the max-cut and traveling salesman problem and found that it outperforms SA. However, there is no direct study that compares performance across quantum annealing, QAOA, and NNQS.

5.2 Results and Discussion

Performance is shown for each of the datasets, accompanied by error bars representing the unbiased standard error of the mean for each data point. Graphs with problem sizes on the x-axis are plotted with a log scale.

5.2.1 NAE3SAT

Performance by size for the NAE3SAT dataset in Figure 5.1 and average performance is shown in Figure 5.2. The D-wave solver and NNQS could both solve problems up to $n = 300$. However, multiple embedding requests were required for problems of size 300 for the D-wave Pegasus topology which suggests that $n = 300$ might be near the D-wave size limit for the NAE3SAT problem. QAOA was only able to solve problems of up to $n = 30$ due to the limitations on the number of qubits of the simulator.

In terms of performance, the D-wave solver performs well up to $n = 50$ with a success probability of 1. For larger problem sizes, the performance of the D-wave solver drops off sharply. The NNQS performs well up to $n = 20$, and then the success probability and normalized energy gradually decline until $n = 300$. The QAOA solver performs well up

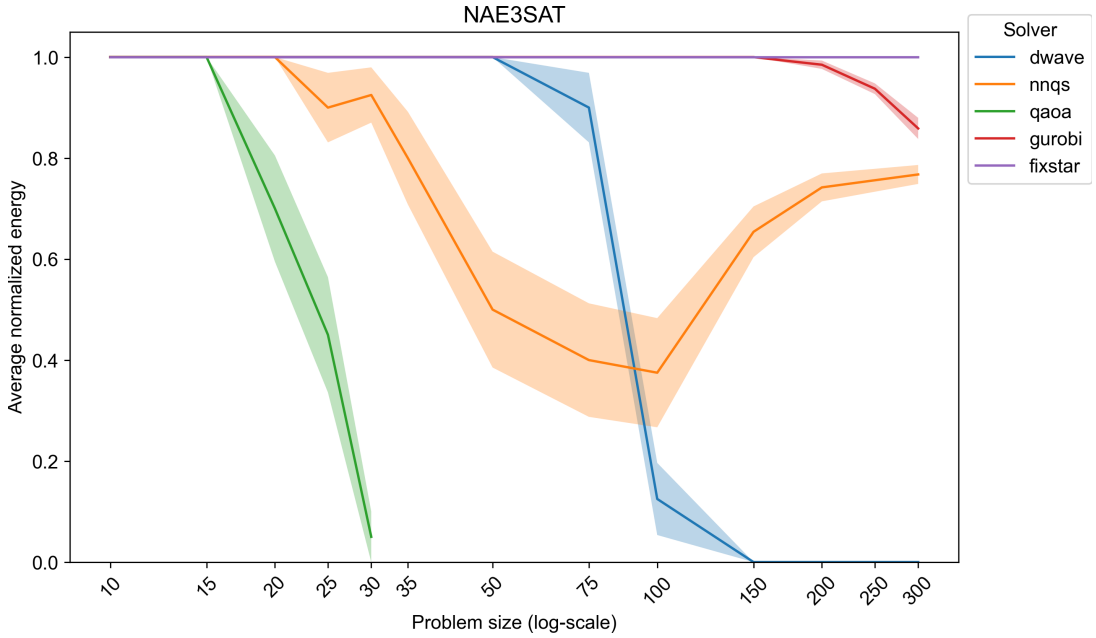

(a) Normalized energy

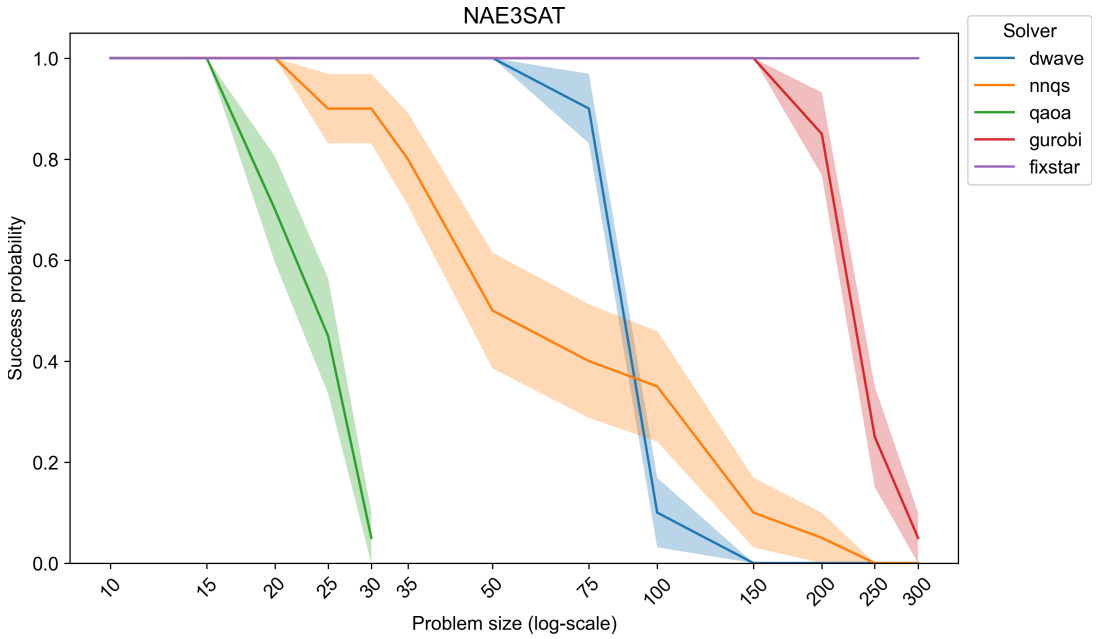

(b) Success probability

Figure 5.1: Performance of different solvers for NAE3SAT by problem size

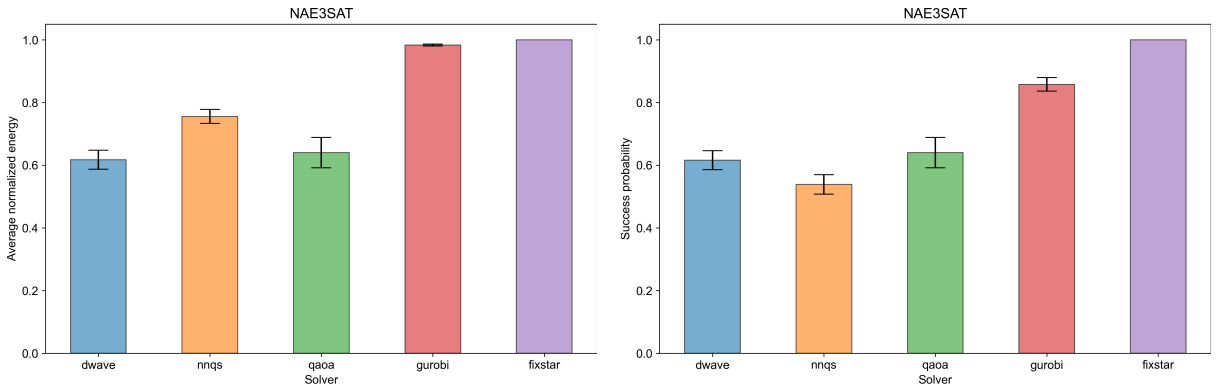

(a) Normalized energy

(b) Success probability

Figure 5.2: Average performance of different solvers for NAE3SAT

to $n = 15$, with declining performance until $n = 30$. Between the classical solvers, the Fixstars QUBO solver performs better than the GUROBI optimizer at larger problem sizes (> 150).

Overall, the NNQS has the highest average normalized energy among the 3 quantum-inspired solvers but has the lowest success probability. This is likely due to it being able to solve problems of larger sizes that the D-wave Annealer and QAOA solver cannot handle.

5.2.2 Max-cut

Performance by size for the max-cut dataset is shown in Figure 5.3 and average performance is shown in Figure 5.4. For the max-cut problem, the D-wave solver could only handle problem sizes up to $n = 150$ due to the need for minor embedding onto the pegasus topology. QAOA was able to solve problems of up to $n = 30$ due to the limitations of the simulator.

In terms of performance, the D-wave solver performs well up to $n = 30$ and the performance drops off sharply for larger problems. The NNQS performs well up to $n = 150$, although the success probability declines for sizes more than 50. The QAOA solver performs well only for $n = 10$, with performance declining afterward.

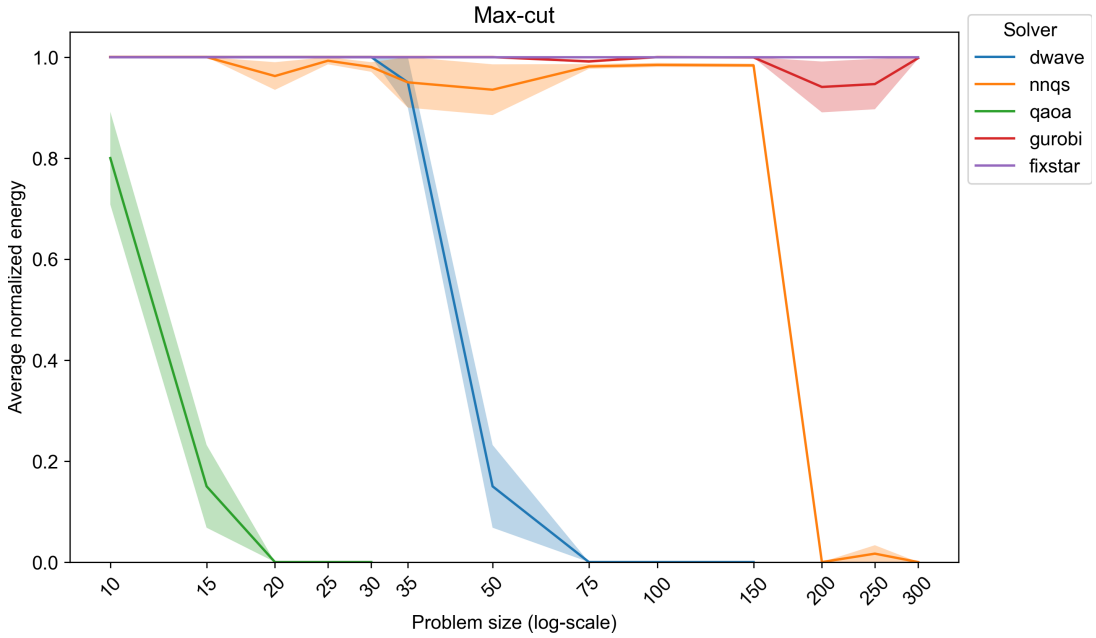

(a) Normalized energy

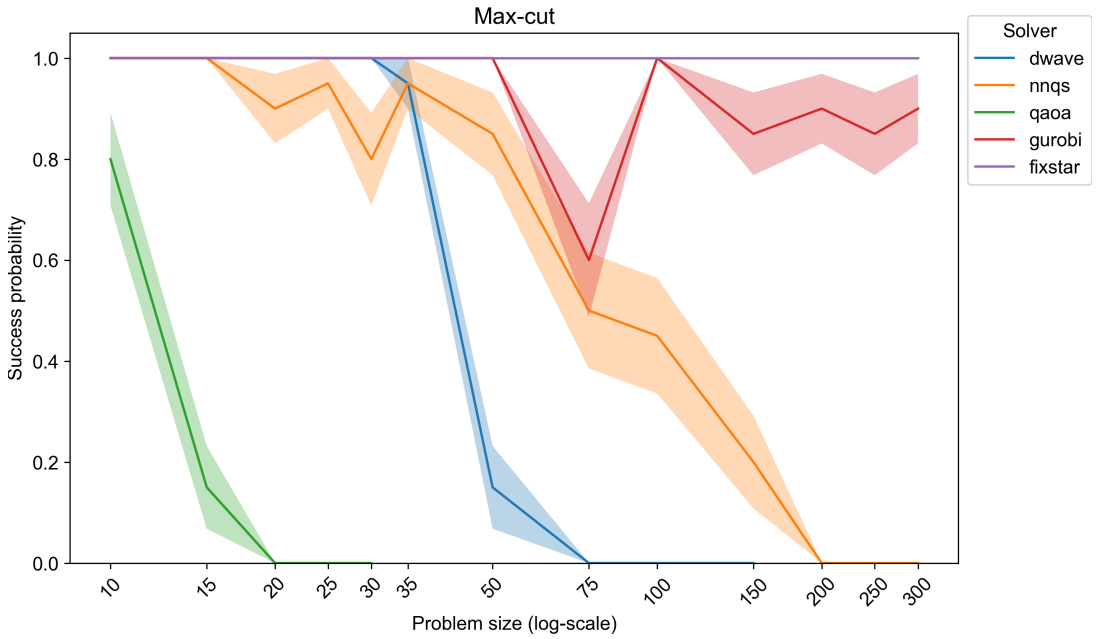

(b) Success probability

Figure 5.3: Performance of different solvers for max-cut by problem size

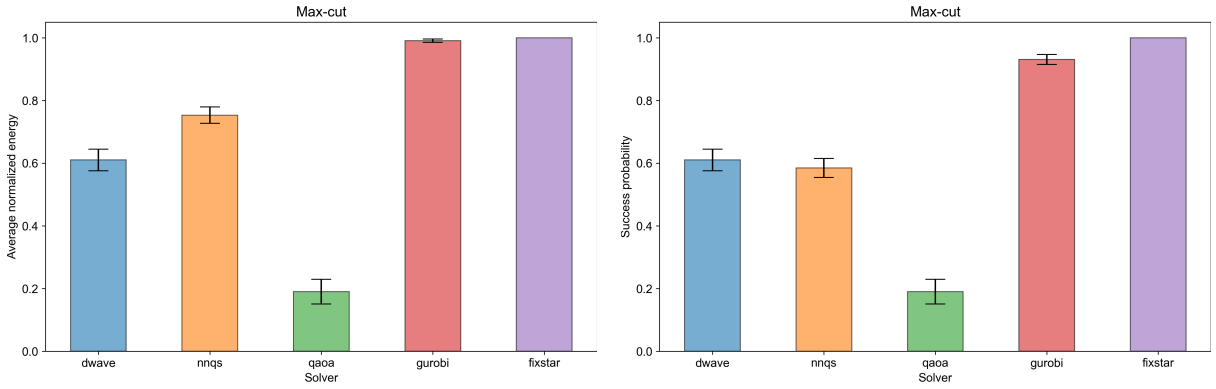

(a) Normalized energy

(b) Success probability

Figure 5.4: Average performance of different solvers for max-cut

Overall, the NNQS has the highest average normalized energy among the 3 quantum-inspired solvers and has similar a success probability as the D-wave solver. The QAOA solver performs poorly in both metrics.

5.2.3 SK model

Performance by size for the SK model dataset is shown in Figure 5.5 and average performance is shown in Figure 5.6. For the SK model, the D-wave solver could only handle problem sizes up to $n = 150$ due to the need for minor embedding onto the pegasus topology. The SK model is fully connected which makes embedding difficult for the D-wave QPU. QAOA was able to solve problems of up to $n = 30$ due to the limitations of the simulator.

The SK model presents a difficult problem for all QUBO solvers due to its multi-valley energy landscape and performance is much less consistent. The D-wave solver performs well up to $n = 30$, with performance gradually decreasing for larger problems. The NNQS follows a similar trend, although it can solve problems of larger sizes and performs better at sizes of $= 100, 150$. The QAOA solver has consistently poor performance across problem sizes.

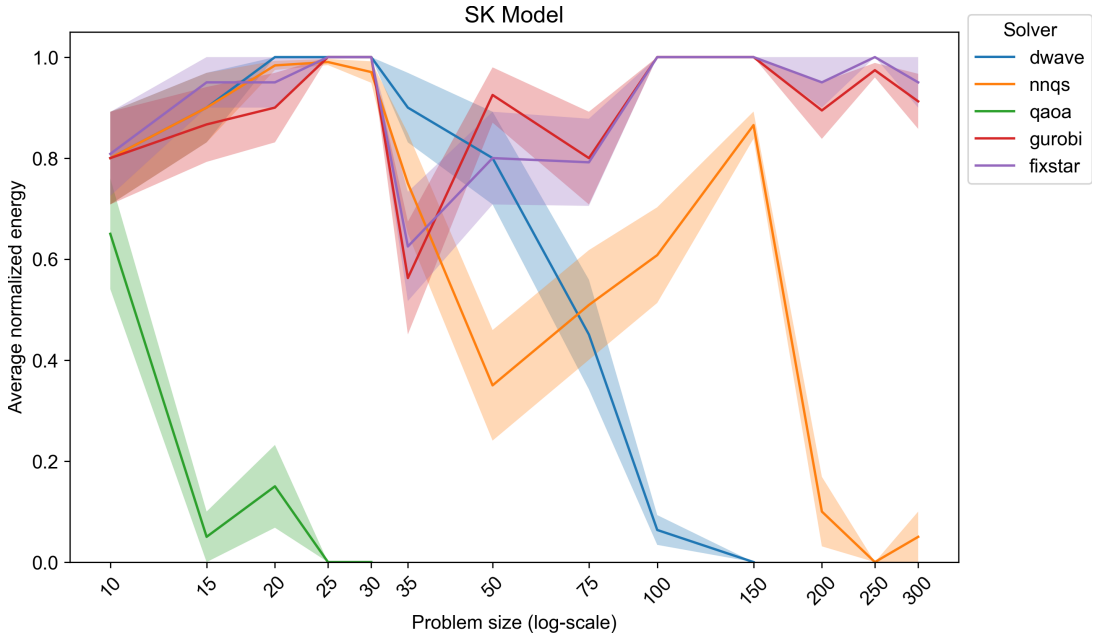

(a) Normalized energy

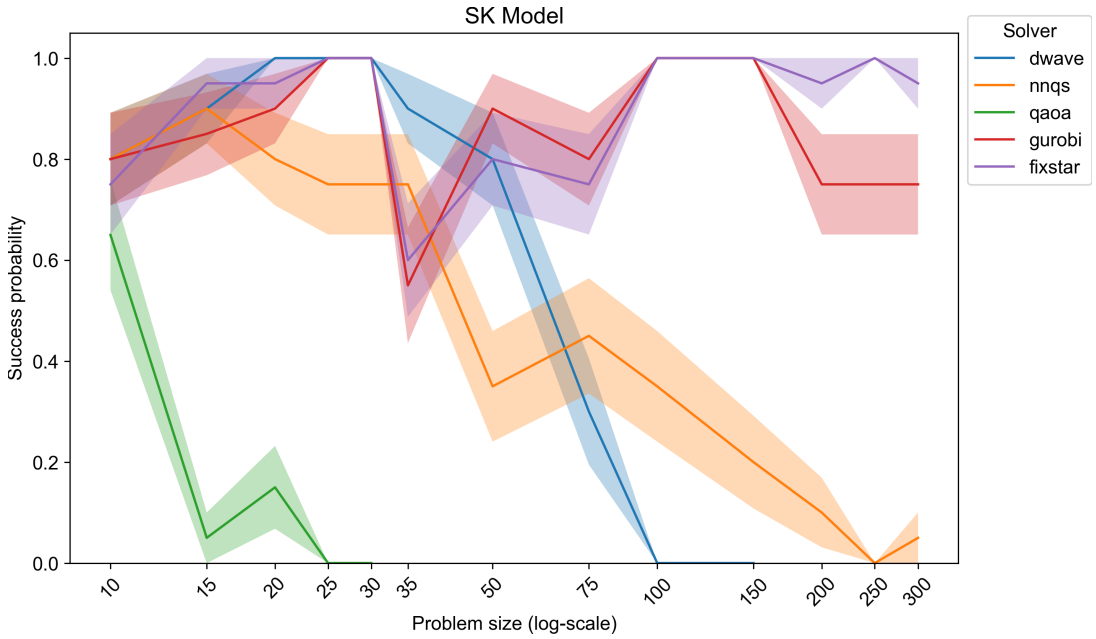

(b) Success probability

Figure 5.5: Performance of different solvers for SK model by problem size

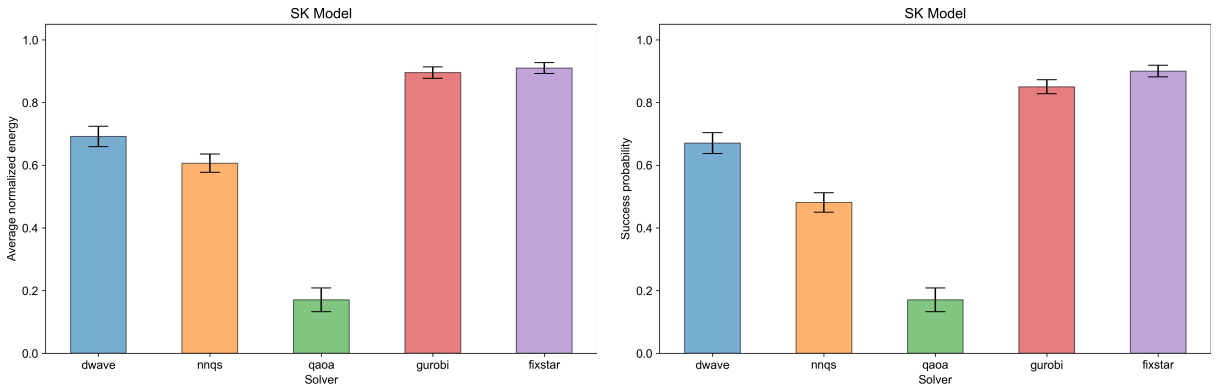

(a) Normalized energy

(b) Success probability

Figure 5.6: Average performance of different solvers for SK model

Overall, the D-wave annealer has the highest average normalized energy and success probability among the 3 quantum-inspired solvers. The NNQS is slightly worse in both metrics while the QAOA solver performs poorly in both metrics.

5.3 Conclusion

When comparing the 3 quantum-inspired solvers, NNQS has the best normalized energy for the NAE3SAT and max-cut dataset while the D-wave solver has the best normalized energy for the SK model performance. NNQS also does the best in normalized energy when averaged across the 3 datasets.

QAOA has the best success probability for the NAE3SAT dataset. However, it is important to note that it was only able to handle problems with up to 30 variables. The D-wave solver has the best success probability for the max-cut and SK model datasets and the success probability averaged across the 3 datasets.

Table 5.1 and Table 5.2 show the average normalized energy and success probability for different solvers for each dataset and the average across all datasets.

	D-wave	NNQS	QAOA	GUROBI	Fixstar
NAE3SAT	0.617	**0.755**	0.640	0.983	1.00
Max-cut	0.610	**0.783**	0.190	0.983	1.00
SK model	**0.691**	0.646	0.178	0.870	0.910
Average	0.640	**0.728**	0.336	0.946	0.970

Table 5.1: Average normalized energy for different solvers

	D-wave	NNQS	QAOA	GUROBI	Fixstar
NAE3SAT	0.617	**0.755**	0.640	0.983	1.00
Max-cut	0.610	**0.783**	0.190	0.983	1.00
SK model	**0.691**	0.646	0.178	0.870	0.910
Average	0.640	**0.728**	0.336	0.946	0.970

Table 5.2: Success probability for different solvers

Chapter 6

NNQS exploration

This chapter explores the effects of different architectures and training schemes that can be used for training NNQS to solve QUBO problems. All experiments in this section were run on a subset of the full dataset with problem sizes of $10, 25, 50, 75, 200, 250$ and 10 problems for each problem type and size. The problem evaluation metrics are also calculated by considering the solutions from the different types of NNQS to be able to draw a clearer comparison between architectures and training schemes.

6.1 Architectures and training algorithms

We will utilize both the Restricted Boltzmann Machine (RBM) and the Multilayer Perceptron (MLP) in their performance as a NNQS. For a given input problem with n variables, the RBM model will have n visible nodes and $5n$ hidden nodes while the MLP will have n input nodes, 1 hidden layer of size $5n$ and 1 positive real output node. The RBM uses the sigmoid function while the MLP uses the ReLU activation function. We use Gibbs sampling for the RBM and Metropolis-Hasting sampling for the MLP, both sampling methods are detailed in section 2.5.

We will also compare 3 training algorithms for NNQS—progressive, direct, and con-

tinuous. The progressive training algorithm follows Algorithm 1. In direct training, the normalized anneal fraction s is held constant at 1 for all epochs and follows Algorithm 2. In continuous training, the NNQS is not trained to convergence but is trained for a single epoch while incrementing the normalized anneal fraction slowly described in Algorithm 3.

Algorithm 2 NNQS Direct Training

Require: Problem Hamiltonian $\hat{H}_c$

Ensure: Trained NNQS

Initialize NNQS with random weights;

Set $H \leftarrow B(1)\hat{H}_c$;

Train NNQS on H until convergence or until epoch limit of 1000 is reached;

Algorithm 3 NNQS Continuous Training

Require: Problem Hamiltonian $\hat{H}_c$

Ensure: Trained NNQS

Initialize NNQS with random weights;

for $s \in [0.001, 1.0]$ step 0.001 **do**

Set $H(s) \leftarrow A(s)\hat{H}_0 + B(s)\hat{H}_c$;

Train NNQS on $H(s)$ for 1 epoch;

Direct training serves as a baseline for directly training a neural network with the cost function as the problem Hamiltonian. Progressive training most closely resembles the quantum annealing process, where the system is kept at the ground state by training until convergence in each increment of s. Continuous training is a combination of the other two by slowly incrementing s but never reaching convergence.

6.2 Results and Discussion

Performance is shown for each of the datasets, accompanied by error bars representing the unbiased standard error of the mean for each data point. Graphs with problem sizes on the x-axis are plotted with a log scale. The graphs for performance by size are shown in Appendix C.

6.2.1 NAE3SAT

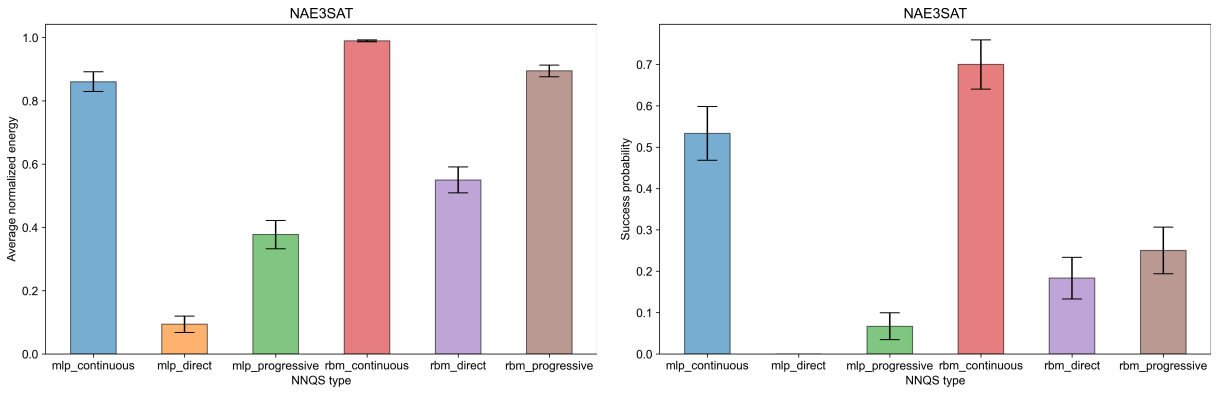

(a) Normalized energy

(b) Success probability

Figure 6.1: Average performance of different NNQS types for NAE3SAT

For the NAE3SAT dataset, the continuous training algorithm with the RBM performs the best in terms of both average performance and success probability when averaged across all sizes, shown in Figure 6.1. In the performance by problem size, the continuous training algorithm with the RBM performed the best in terms of normalized energy and success probability, shown in Figure C.1, except with a problem size of 50. This is likely due to variance in the randomly generated data set.

6.2.2 Max-cut

For the maxcut dataset, the continuous training algorithm with the RBM performs the best in terms of both average performance and success probability when averaged across

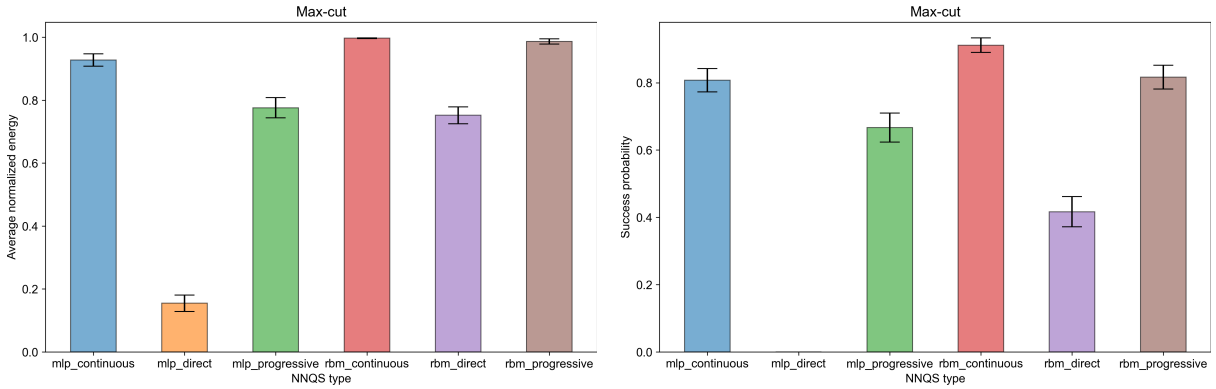

(a) Normalized energy

(b) Success probability

Figure 6.2: Average performance of different NNQS types for max-cut

all sizes, shown in Figure 6.2. In the performance by problem size, the continuous training algorithm with the RBM performed the best in terms of normalized energy and success probability, shown in Figure C.2, except with a problem size of 25. This is likely due to variance in the randomly generated data set. However, the gap in success probability between the models is relatively small and this likely implies that the max-cut problem is easier in general compared to the NAE3SAT problem.

6.2.3 SK model

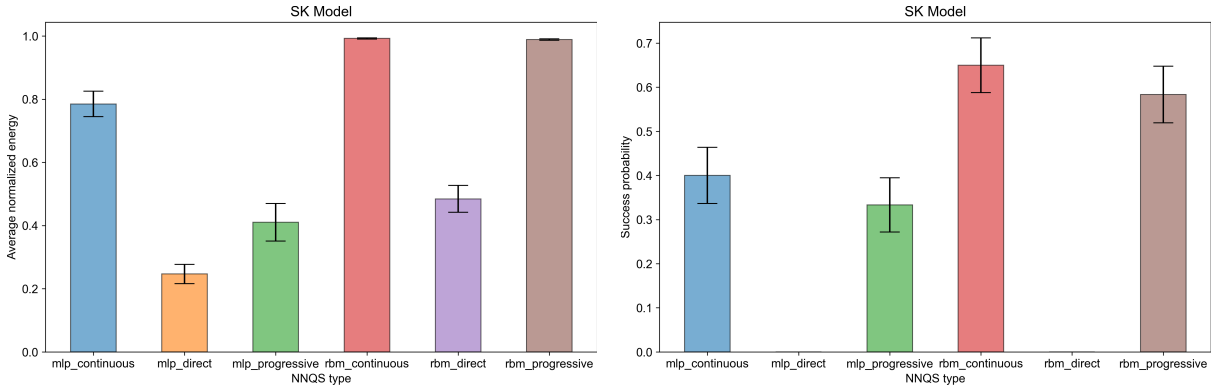

(a) Normalized energy

(b) Success probability

Figure 6.3: Average performance of different NNQS types for SK model

For the SK model dataset, the continuous training algorithm with the RBM performs the best in terms of both average performance and success probability when averaged across all sizes, shown in Figure 6.3. The performance averaged across all sizes, shown in Figure 6.3, also highlights that the RBM with a continuous training algorithm performs the best. However, it is interesting that the direct training schemes have poor performance with small problem sizes (≤ 50) but are relatively better at higher problem sizes $(100, 250)$.

6.3 Conclusion

Across all the problem sets, the RBM has a better average performance compared to the MLP in both average normalized energy and success probability for each training algorithm. In terms of training schemes, direct training performs the worst among the 3, and continuous training performs better than progressive training. Using the RBM with a continuous training scheme gives the highest normalized energy and success probability across all datasets.

Table 6.1 and Table 6.2 show the average normalized energy and success probability for different types of NNQS for each dataset and the average across all datasets.

	MLP			RBM		
	Continuous	Direct	Progressive	Continuous	Direct	Progressive
NAE3SAT	0.860	0.087	0.349	**0.990**	0.508	0.895
Max-cut	0.928	0.155	0.776	**0.997**	0.752	0.987
SK model	0.785	0.247	0.410	**0.992**	0.484	0.989
Average	0.858	0.163	0.512	**0.993**	0.581	0.957

Table 6.1: Average normalized energy for different NNQS types

	MLP			RBM		
	Continuous	Direct	Progressive	Continuous	Direct	Progressive
NAE3SAT	0.533	0.000	0.062	**0.700**	0.167	0.227
Max-cut	0.808	0.000	0.667	**0.912**	0.417	0.817
SK model	0.400	0.000	0.333	**0.650**	0.000	0.583
Average	0.580	0.000	0.354	**0.754**	0.194	0.542

Table 6.2: Success probability for different NNQS types

Chapter 7

Conclusion

This chapter summarises the contributions and limitations of our study. There are also recommendations for further work that could be investigated by future projects.

7.1 Contributions

In this study, we have benchmarked 5 QUBO solvers:

1. D-Wave Quantum Annealing
2. Neural Network Quantum States (NNQS)
3. Quantum Approximate Optimization Algorithm (QAOA)
4. GUROBI Optimizer
5. Fixstars Amplify QUBO Solver

3 datasets were used which comprised of 3 types of combinatorial optimization problems:

1. Not-all-equal 3-satisfiability (NAE3SAT)
2. Max-cut

3. Sherrington-Kirkpatrick model (SK model)

Among the quantum-inspired solvers, our results show that the D-wave and NNQS solvers achieve the best performance. The NNQS solver is generally better than the D-wave solver except for the SK model dataset. The QAOA solver achieves generally poor performance across datasets and is not comparable due to the lack of large-scale gate-based quantum computers. All 3 quantum-inspired solvers underperform the 2 classical solvers with the simulatedannealingbased Fixstar Amplify QOBO solver achieving the best performance out of all solvers for all datasets.

We also investigated the NNQS solver with different architectures and training algorithms. The Restricted Boltzmann Machine (RBM) and the Multilayer Perceptron (MLP) were used as the underlying neural networks along with 3 different training algorithms—progressive, direct, and continuous. We found that using the RBM with a continuous training scheme gives the best performance across all datasets.

The main limitation of the study was for the QAOA solver which was from the limited access to a working gate-based quantum computer from IBMQ. This meant that we had to use the simulator instead which could only handle up to 30 variables. However, as the QAOA simulator does not model quantum noise and the results from the QAOA solver for small problems are not promising, QAOA on a real quantum device would perform even worse for larger problems and is thus not interesting to test in the current NISQ era. The other significant limitation was that the NNQS exploration dataset was relatively smaller due to runtime constraints. However, as there were still 60 problems for each solver, the standard error for performance was small.

7.2 Future work

Future studies can explore more QUBO problem types and attempt to classify classes of problems that are difficult for annealing-based solvers such as QA and SA but easier for

other solvers such as QAOA. When gate-based quantum computers are readily available, the QAOA solver with higher $p > 1$ values could be benchmarked which should give better performance.

For further work with NNQS, future studies could investigate if more modern machine learning models such as Graph Neural Networks or Attention-based Neural Networks can be used as the underlying architecture for NNQS and whether they provide better performance.

Future work could also investigate whether NNQS closely approximates the wave function of a D-wave solver in the quantum annealing process. This could be done by conducting a quench of the D-wave annealing process in order to take a snapshot of the intermediate state. Some initial work is detailed in Appendix B but has not been included in the main report as the results are not substantial.

References

Achlioptas, D., Chtcherba, A., Istrate, G., & Moore, C. (2001). The phase transition in 1-in-k sat and nae 3-sat. *Proceedings of the Annual ACM-SIAM Symposium on Discrete Algorithms*, , , 05, 2001.

Alidaee, B. (2009). Minimizing absolute and squared deviation of completion times from due dates. *Production and Operations Management*, *3*, , 01, 2009, 133 – 147.

Alidaee, B., Glover, F., Kochenberger, G., & Rego, C. (2005). A new modeling and solution approach for the number partitioning problem. *JAMDS*, *9*, , 01, 2005, 113–121.

Barahona, F. (1982). On the computational complexity of ising spin glass models. *Journal of Physics A: Mathematical and General*, *15*(10), , 1982, 3241.

Baxter, R. J. (2016). *Exactly solved models in statistical mechanics*. Elsevier.

Blekos, K., Brand, D., Ceschini, A., Chou, C.-H., Li, R.-H., Pandya, K., & Summer, A. (2023). A Review on Quantum Approximate Optimization Algorithm and its Variants.

Born, M., & Fock, V. (1928). Beweis des adiabatensatzes. *Zeitschrift für Physik A Hadrons and Nuclei*, *51*, , 03, 1928, 165–180.

Carleo, G., & Troyer, M. (2017). Solving the quantum many-body problem with artificial neural networks. *Science*, *355*, , 02, 2017, 602.

Cipra, B. A. (1987). An introduction to the ising model. *The American Mathematical Monthly*, *94*(10), , 1987, 937–959.

D. J. Thouless, P. W. A., & Palmer, R. G. (1977). Solution of 'solvable model of a spin glass'. *The Philosophical Magazine: A Journal of Theoretical Experimental and Applied Physics*, *35*(3), , 1977, 593–601.

D-Wave Systems (2023). Minor-embedding.

Denchev, V. S., Boixo, S., Isakov, S. V., Ding, N., Babbush, R., Smelyanskiy, V., Martinis, J., & Neven, H. (2016). What is the computational value of finite-range tunneling? *Physical Review X*, *6*(3), , 2016, 031015.

Dunning, I., Gupta, S., & Silberholz, J. (2018). What works best when? a systematic evaluation of heuristics for max-cut and qubo. *INFORMS Journal on Computing*, *30*, , 08, 2018, 608–624.

Farhi, E., Goldstone, J., & Gutmann, S. (2014). A quantum approximate optimization algorithm.

Farhi, E., Goldstone, J., Gutmann, S., Lapan, J., Lundgren, A., & Preda, D. (2001). A quantum adiabatic evolution algorithm applied to random instances of an np-complete problem. *Science*, *292*(5516), , 2001, 472–475.

Farhi, E., & Harrow, A. W. (2016). Quantum supremacy through the quantum approximate optimization algorithm.

Geman, S., & Geman, D. (1984). Stochastic relaxation, gibbs distributions, and the bayesian restoration of images. *IEEE Transactions on pattern analysis and machine intelligence*, *6*, , 1984, 721–741.

Glover, F., Kochenberger, G., Hennig, R., & Du, Y. (2022). Quantum bridge analytics i: a tutorial on formulating and using qubo models. *Annals of Operations Research*, *314*, , 07, 2022.

Gomes, J., McKiernan, K. A., Eastman, P., & Pande, V. S. (2019). Classical quantum optimization with neural network quantum states. *arXiv preprint arXiv:1910.10675*, , , 2019.

Griffiths, D. J., & Schroeter, D. F. (2018). *Introduction to quantum mechanics*. Cambridge University Press, 3 edition.

Gurobi Optimization, LLC (2023). Gurobi Optimizer Reference Manual.

Harris, R., Sato, Y., Berkley, A., Reis, M., Altomare, F., Amin, M., Boothby, K., Bunyk, P., Deng, C., Enderud, C., Huang, S., Hoskinson, E., Johnson, M., Ladizinsky, E., Ladizinsky, N., Lanting, T., Li, R., Medina, T., Molavi, R., & Yao, J. (2018). Phase transitions in a programmable quantum spin glass simulator. *Science (New York, N.Y.)*, *361*, , 07, 2018, 162–165.

Hastings, W. K. (1970). Monte carlo sampling methods using markov chains and their applications. *Biometrika*, *57*(1), , 1970, 97–109.

Horn, R. A., & Johnson, C. R. (1990). *Matrix analysis*. Cambridge University Press.

IBM (2024).

Inc., D.-W. S. (2024a).

Inc., D.-W. S. (2024b).

Ising, E. (1925). Beitrag zur theorie des ferromagnetismus. *Zeitschrift für Physik*, *31*(1), , 1925, 253–258.

Kadowaki, T., & Nishimori, H. (1998). Quantum annealing in the transverse ising model. *Physical Review E*, *58*(5), , 1998, 5355.

Katayama, K., & Narihisa, H. (2001). Performance of simulated annealing-based heuristic for the unconstrained binary quadratic programming problem. *European Journal of Operational Research*, *134*(1), , 2001, 103–119.

Khandoker, S. A., Abedin, J. M., & Hibat-Allah, M. (2023). Supplementing recurrent neural networks with annealing to solve combinatorial optimization problems. *Machine Learning: Science and Technology*, *4*(1), , 2023, 015026.

Kirkpatrick, S., Gelatt, C. D., & Vecchi, M. P. (1983). Optimization by simulated annealing. *Science*, *220*(4598), , 1983, 671–680.

Kochenberger, G., Hao, J.-K., Glover, F., Lewis, M., Lu, Z., Wang, H., & Wang, Y. (2014). The unconstrained binary quadratic programming problem: A survey. *Journal of Combinatorial Optimization*, *28*, , 07, 2014.

Kochenberger, G., Hao, J.-K., Lu, Z., Wang, H., & Glover, F. (2013). Solving large scale max cut problems via tabu search. *Journal of Heuristics*, *19*, , 08, 2013.

Kolmogorov, A. N. (1957). On the representation of continuous functions of many variables by superposition of continuous functions of one variable and addition. *Doklady Akademii Nauk*, Vol. 114 (pp. 953–956), Russian Academy of Sciences, , 1957.

Kramers, H. A., & Wannier, G. H. (1941). Statistics of the two-dimensional ferromagnet. part i. *Phys. Rev.*, *60*, , Aug, 1941, 252–262.

Kurowski, K., Pecyna, T., Slysz, M., Rozycki, R., Waligora, G., & Weglarz, J. (2023). Application of quantum approximate optimization algorithm to job shop scheduling problem. *European Journal of Operational Research*, *310*, , 03, 2023.

Lanczos, C. (1950). An iteration method for the solution of the eigenvalue problem of linear differential and integral operators. *J. Res. Natl. Bur. Stand. B*, *45*, , 1950, 255–282.

Lang, J., Zielinski, S., & Feld, S. (2022). Strategic portfolio optimization using simulated, digital, and quantum annealing. *Applied Sciences*, *12*(23), , 2022.

Lehoucq, R., Sorensen, D., & Yang, C. (1998). *Arpack users' guide: Solution of large-scale eigenvalue problems with implicitly restarted arnoldi methods*. Software, Environments, and Tools. Society for Industrial and Applied Mathematics.

Lucas, A. (2014). Ising formulations of many np problems. *Frontiers in Physics*, *2*, , 02, 2014, 5.

McGeoch, C., & Farré, P. (2021). *The advantage system: Performance update* (Technical report). D-Wave Systems.

Onsager, L. (1944). Crystal statistics. i. a two-dimensional model with an order-disorder transition. *Phys. Rev.*, *65*, , Feb, 1944, 117–149.

Palubeckis, G. (2006). Iterated tabu search for the unconstrained binary quadratic optimization problem. *Informatica*, *17*(2), , apr, 2006, 279–296.

Pelofske, E., Bärtschi, A., & Eidenbenz, S. (2023). Quantum annealing vs. qaoa: 127 qubit higher-order ising problems on nisq computers. In A. Bhatele, J. Hammond, M. Baboulin, & C. Kruse (Eds.), *High Performance Computing* (pp. 240–258), , 2023: Springer Nature Switzerland.

Punnen, A. P. (2022). *The quadratic unconstrained binary optimization problem*. Springer International Publishing.

Qiskit contributors (2023). Qiskit: An open-source framework for quantum computing.

Quintero, R., & Zuluaga, L. (2022). Qubo formulations of combinatorial optimization problems for quantum computing devices.

Rieffel, E., Venturelli, D., O'Gorman, B., do, M., Prystay, E., & Smelyanskiy, V. (2014). A case study in programming a quantum annealer for hard operational planning problems. *Quantum Information Processing*, *14*, , 07, 2014.

Rosenberg, G., Haghnegahdar, P., Goddard, P., Carr, P., Wu, J., & Lopez de Prado, M. (2016). Solving the optimal trading trajectory problem using a quantum annealer. *IEEE Journal of Selected Topics in Signal Processing*, *10*, , 09, 2016, 1–1.

Tavares, G. (2008). *New algorithms for quadratic unconstrained binary optimization (qubo) with applications in engineering and social sciences*. PhD thesis, Rutgers University.

Willsch, M., Willsch, D., Jin, F., De Raedt, H., & Michielsen, K. (2020). Benchmarking the quantum approximate optimization algorithm. *Quantum Information Processing*, *19*(7), , Jun, 2020, 197.

Yarkoni, S., Huck, A., Schuelldorf, H., Speitkamp, B., Tabrizi, M., Leib, M., Back, T., & Neukart, F. (2021). *Solving the shipment rerouting problem with quantum optimization techniques*, pp. 502–517. Springer, Cham.

Yarkoni, S., Raponi, E., Back, T., & Schmitt, S. (2022). Quantum annealing for industry applications: Introduction and review. *Reports on Progress in Physics*, *85*, , 08, 2022.

Zen, R. A. M. (2021). *Transfer learning for neural-network quantum states*. PhD thesis, National University of Singapore. Available at `https://scholarbank.nus.edu.sg/handle/10635/224567`.

Zen, R. A. M., My, L., Tan, R., Hébert, F., Gattobigio, M., Miniatura, C., Poletti, D., & Bressan, S. (2020). Finding quantum critical points with neural-network quantum states. *European Conference on Artificial Intelligence*, , 2020.

Zhou, L., Wang, S.-T., Choi, S., Pichler, H., & Lukin, M. D. (2020). Quantum approximate optimization algorithm: Performance, mechanism, and implementation on near-term devices. *Phys. Rev. X*, *10*, , Jun, 2020, 021067.

Appendix A

Curve fitting for NNQS

This section will describe how we obtained an approximate analytical form of functions $A(s)$ and $B(s)$ as shown in Figure 4.2. The exact form is not provided in the D-wave documentation but a set of 1000 points is available from the documentation (Inc., 2024b). A snapshot of the dataset is shown here:

s	$A(s)$ (GHz)	$B(s)$ (GHz)
0	0.000000	9.839417×10^{0}
0.001	0.001001	9.746483×10^{0}
0.002	0.002002	9.655434×10^{0}
...	...	...
0.998	0.997998	1.344913×10^{-9}
0.999	0.998999	1.293784×10^{-9}
1.000	1.000000	1.242656×10^{-9}

Table A.1: Discrete points of annealing functions $A(s)$ and $B(s)$.

To obtain an analytical form, we utilised the curve fit function from the scipy library. First, we normalize by the maximum value in $B(s)$ as only the ratio of A and B is We fit an exponential decay form of $a_A \cdot e^{-b_A \cdot s} + c_A$ to $A(s)$ and a quadratic function $a_B \cdot s^2 + b_B \cdot s + c_B$

function to $B(s)$. The forms of the functions were chosen from the D-wave documentation (Inc., 2024b). We obtain fitted constants of $a_A = 1.11, b_A = 7.06, c_A - 0.00569, a_B = 0.680, b_B = 0.288, c_B = 0.0305$. The fitted functions are shown in Figure A.1 along with the discrete values from the documentation and are found to be a good fit.

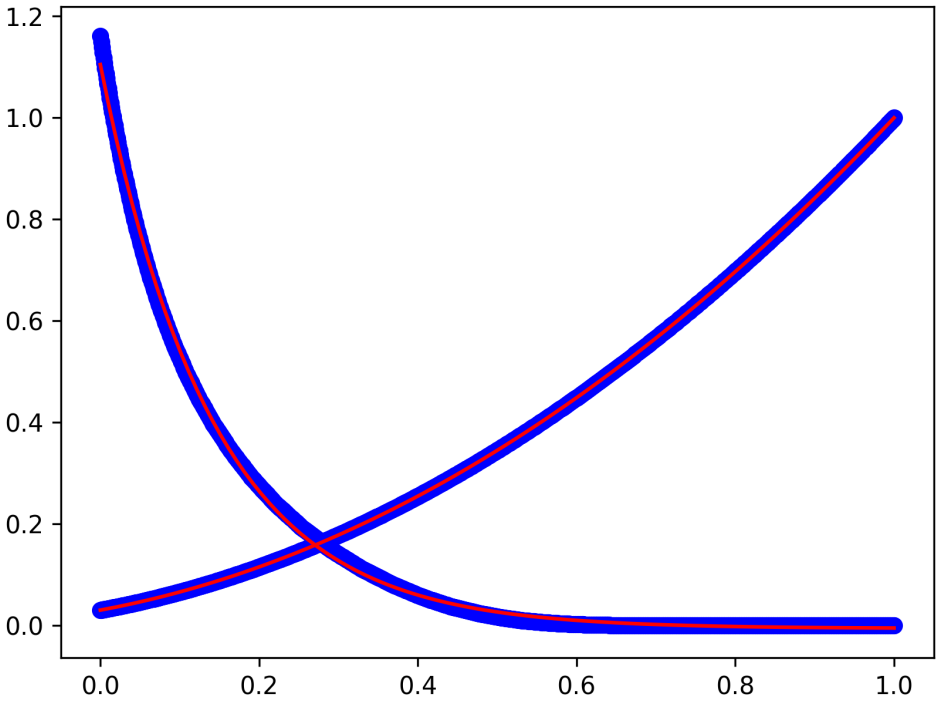

Figure A.1: Fitted $A(s)$ and $B(s)$ equations (red) with discrete values (blue) against the normalized annealing fraction s.

Appendix B

D-wave Quenching

A mid-anneal quench helps us identify the current state of the D-wave annealing by quickly increasing the value of s, the anneal fraction. By doing so, we change the system quickly compared to the system which does not give the system enough time to evolve which freezes the current state. By then measuring the distribution of states through repeated sampling, we can peek into the evolution of the wave function of the D-wave annealing setup and compare it to that of the NNQS.

We can quench the annealing process in a D-wave solver by specifying the anneal_schedule parameter by providing discrete points for (anneal fraction, time) (McGeoch & Farré, 2021). For example, a schedule that is $[(0.0, 0.0)(10.0, 0.5)(11.0, 1.0)]$, would mean a $10\mu s$ anneal until $s = 0.5$ then a $1\mu s$ quench until $s = 1$.

Appendix C

NNQS exploration performance by sizes

C.1 NAE3SAT

Refer to Figure C.1.

C.2 Max-cut

Refer to Figure C.2.

C.3 SK model

Refer to Figure C.3.

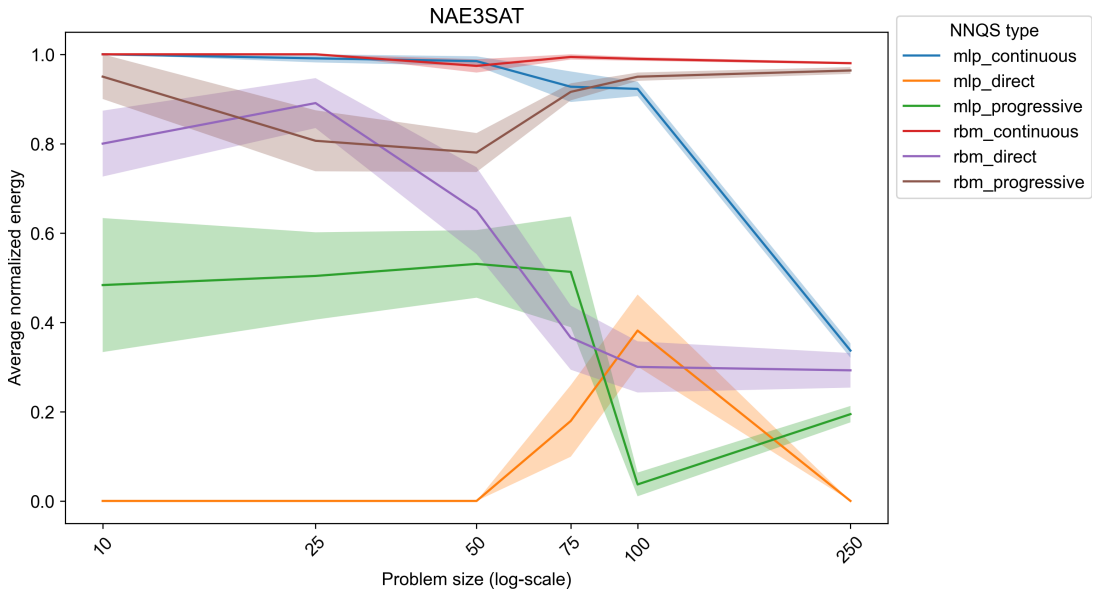

(a) Normalized energy

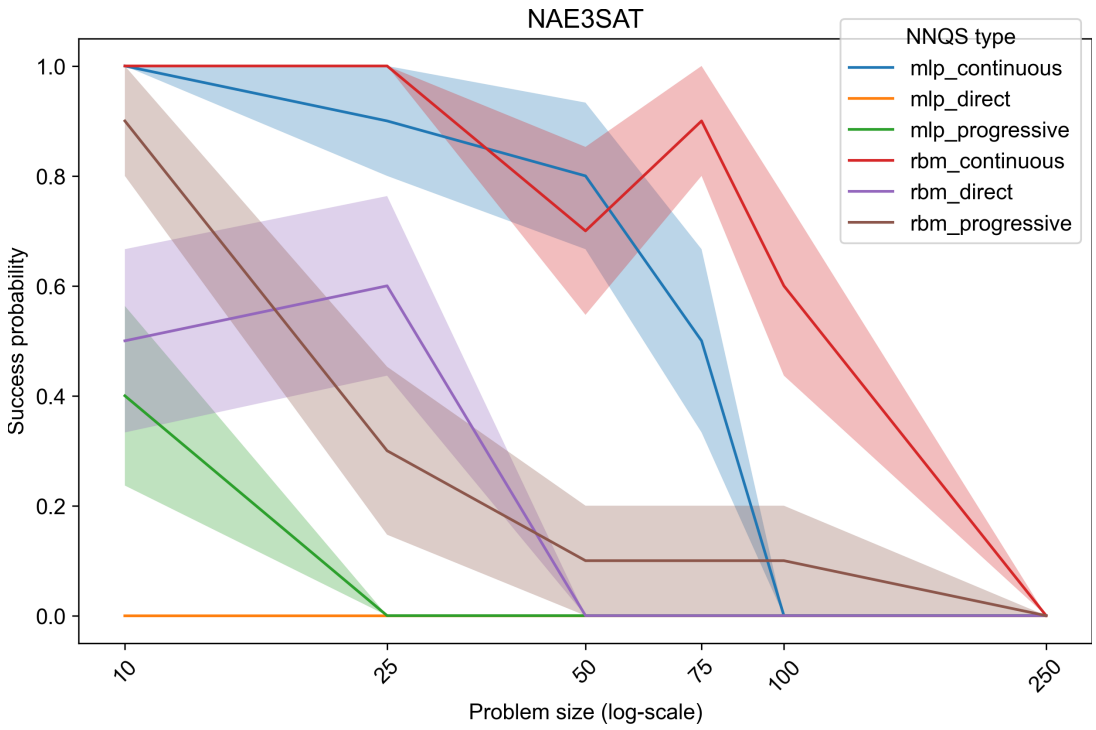

(b) Success probability

Figure C.1: Performance of different NNQS types for NAE3SAT by problem size

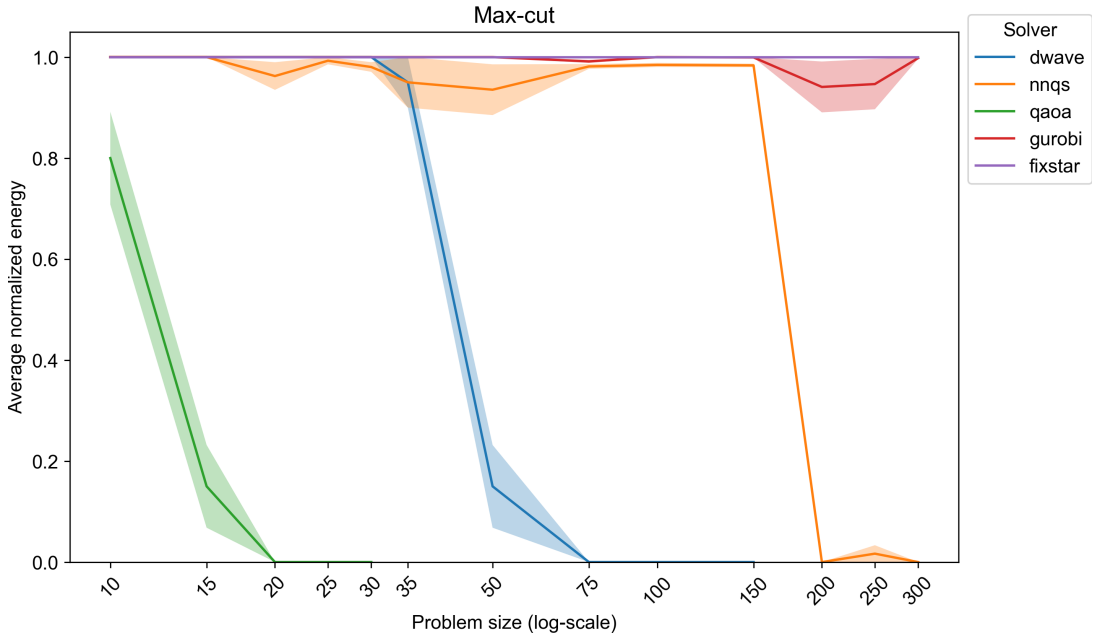

(a) Normalized energy

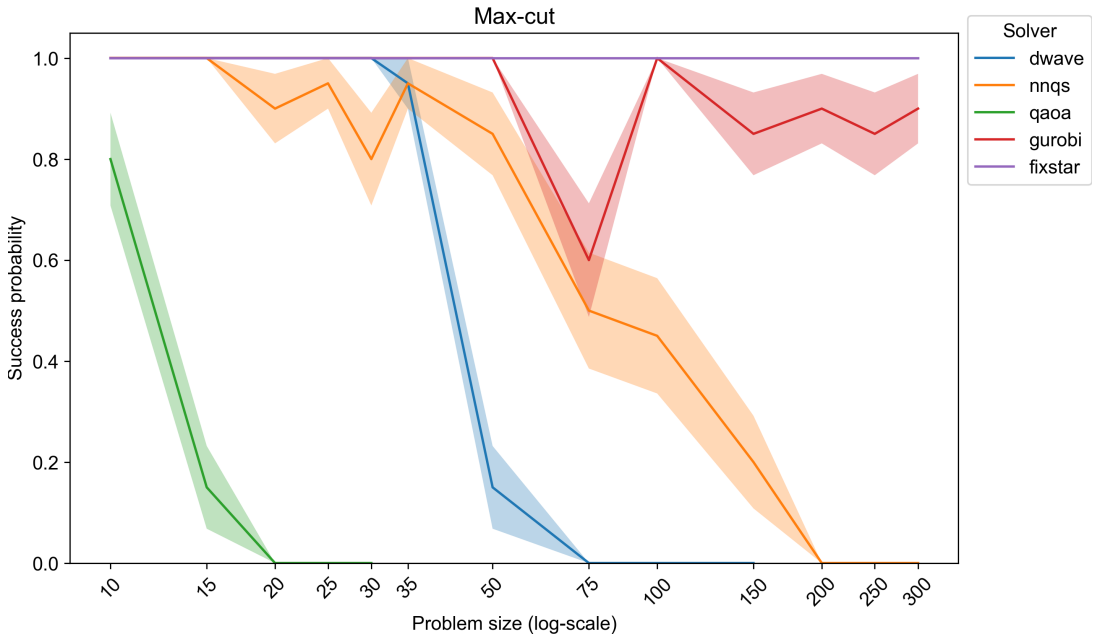

(b) Success probability

Figure C.2: Performance of different solvers for max-cut by problem size

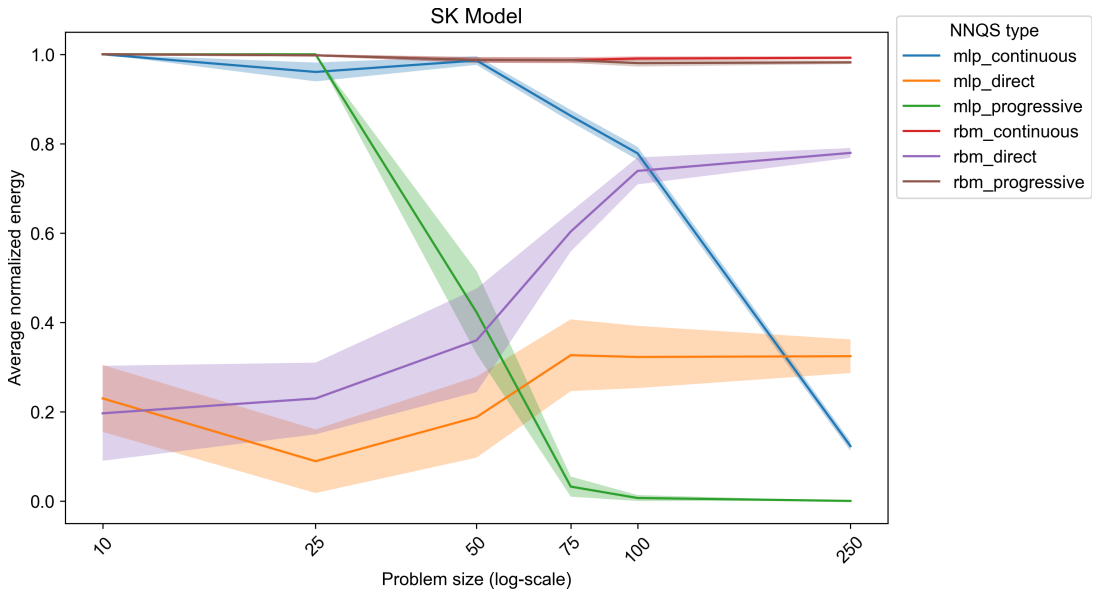

(a) Normalized energy

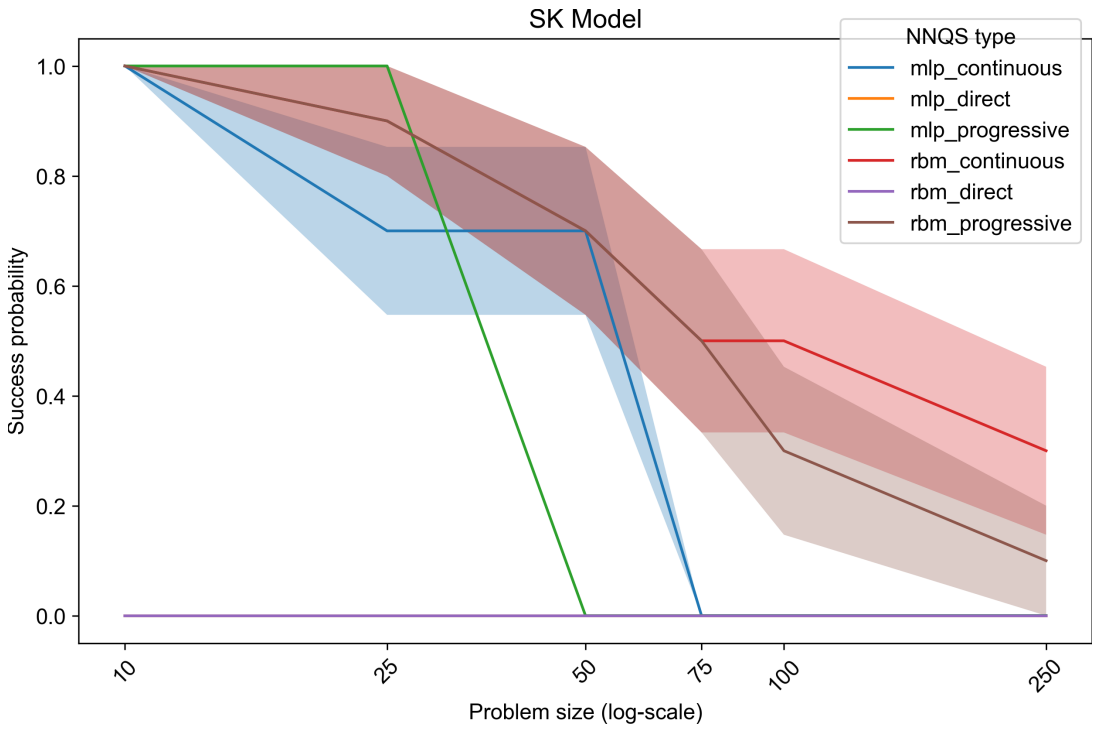

(b) Success probability

Figure C.3: Performance of different NNQS types for SK model by problem size